PRECIPITATION BEHAVIOUR IN NICKEL - 14 ATOM PERCENT SILICON ALLOY

By

VISHVA BANDHU

ME
1986
M
BAN
PRE

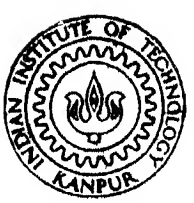

DEPARTMENT OF METALLURGICAL ENGINEERING

INDIAN INSTITUTE OF TECHNOLOGY KANPUR

JUNE 1986

PRECIPITATION BEHAVIOUR IN NICKEL - 14 ATOM PERCENT SILICON ALLOY

A Thesis Submitted

in Partial Fulfilment of the Requirements

for the Degree of

MASTER OF TECHNOLOGY

By

VISHVA BANDHU

to the

DEPARTMENT OF METALLURGICAL ENGINEERING

INDIAN INSTITUTE OF TECHNOLOGY KANPUR

JUNE 1986

23 SEP 1987
CENTRAL LIBRARY
Acc No A. 98040

ME - 1986 - M - BAN - PRE

To

Kumari **Anita Mittal** *[Billa]*

My Love

and

Vikky and Guia,

in the hands of

which the future lies

POST GRADUATE OFFICE
Submitted on 18/6/84

Certificate

Certified that this work on 'Precipitation Behaviour in Ni-14 at. % Si Alloy' by Mr. Vishva Bandhu has been carried out under my supervision and that this has not been submitted elsewhere for a degree.

(Dr. A. K. Jena)
Professor
Department of Metallurgical Engineering
Indian Institute of Technology
Kanpur.

Acknowledgements

I express my hearty gratitude to Professor A.K. Jena for his excellent guidance and constant advice throughout the course of this work. It was a great pleasure working under the guidance of him and I esteem very much the invaluable experience I gained under his supervision.

I am thankful to Mr. V.P. Gupta of Crystal Growth Lab., Mr. K.P. Mukherjee of Physical Metallurgy Lab., Mr. Uma Shankar of X-ray Lab., Mr. V. Kumar of Phase Stability Lab., Mr. B. Jain of Material Testing Lab. and Mr. V.P. Sharma of Electron Microscopic Lab.

My special regards to Mr. Arvind Sharma who helped me a lot in making the computer calculations.

I owe to all of my friends who helped me at various stages of my work.

Finally, my thanks are due to Mr. R.N. Srivastava for typing the manuscript in an elegant form.

- VISHVA BANDHU

Contents

LIST OF TABLES

LIST OF FIGURES

Abstract

The lattice parameter of Ni-14 at. % Si alloy measured by X-ray diffraction was found to be 0.351810 nm. The sample has been aged at 5 different temperatures for various lengths of time and the kinetics of precipitation has been studied by measuring their lattice parameters. The lattice parameter of precipitate phase has been determined at all the 5 temperatures for various lengths of time, it was found to be 0.35022 nm. The solvus line has been determined and the analysis of solvus line gives a value of -351 cal/mole for the standard enthalpy of formation of compound $Ni_{0.773}Si_{0.227}$. The C-curve has been established. The kinetics of precipitation studied in this investigation follows the Johnson-Mehl type of equation. The slope 'n' was found to be 0.83 at all aging times and temperatures which shows that same mechanism is valid at all temperatures and for entire time range. Work on precipitation hardening suggests that the hardening can be observed at temperatures below 650°C. At higher temperatures no appreciable hardening was observed. The precipitation of this alloy could not be suppressed by aircooling. This is due to the low mismatch between solid solution and the precipitate which was only 0.45% found in this investigation.

Chapter I

Introduction

Nickel is the hardest and strongest of the unalloyed common metals with good ductility and malleability.[1] It is a rather chemically inactive metal and characterized by good resistance to corrosion and oxidation. It is white in colour and has good workability and good mechanical properties. It forms tough, ductile solid-solution alloys with many of the common metals. It has wide range of solubilities for other alloying elements. Approximately 60% of the nickel produced is used in stainless and nickel-alloy steels. Most of the remainder is used in high nickel alloys and for electroplating. When one uses nickel as an alloying element, one can achieve several beneficial properties such as greater strength without increase in brittleness, fineness of grain structure, improved fatigue resistance, improved corrosion resistance and resistance to oxidation at higher temperatures and improved strength at higher temperatures.

Nickel base superalloys constitute an important class of materials for high temperature applications at elevated temperatures. Despite their comparative simplicity and binary alloys Ni-Al and Ni-Ti are representative of Nickel-base superalloys because they can also be hardened by coherent precipitation of the γ'-phase.[2] The γ'-phase has the $L1_2$ crystal structure and composition Ni_3X

in the binary alloys (X = Al, Ti, Si). In the commercial alloys a variety of other alloying elements are liberally substitute for nickel and X on their respective sublattices.

The primary interest generated in carrying out this project work is that the silicon forms Ni_3Si with nickel which is face-centered cubic[3,4,5,6] and forms coherently.[7] It was also found that the lattice spacing of the β_1-Ni_3Si phase is smaller than the value of the FCC disordered phase (γ) at corresponding compositions. Similar contraction was observed in the Ni-Ge alloys.[8] This behaviour is in considerable contrast to the results of the Ni-Al and Ni-Ga alloys.[9] In these alloys, it has been shown that the lattice spacing of the γ'-phase with the L_2 structure lie on the extrapolated linear variations of spacing with at. % Al or Ga in the FCC solid solutions. Nevertheless, among the Ni-base binary alloys, the aged Ni-Si alloys have the smallest mismatch between the lattice spacings of the precipitate and the matrix. The lattice misfit is only 0.24%[7,10,11] so that the resulting coherency stresses around the particles which increase the nucleation energy and influence the particle growth are comparatively small. Also due to the small mismatch, the coherent solubility of γ' is probably not much greater than the incoherent solubility.[12] Also the degree of long range order for γ' Ni-Si (23.1 at. % Si) quenched from 1030°C was found to be 0.92 suggests that the two-phase remain highly ordered upto the temperatures close to the limits of solubility[13]

similar to γ'-Ni_3Al. An important feature of the mechanical behaviour of γ'-Ni_3Al is the reversibility of the flow stress upon performing tests at high and low temperatures.[14] For small strains, the flow stress of γ'-Ni_3Al appears solely to be a function of the test temperature. Also γ'-Ni-Si showed similar, reversible flow stress behaviour, entirely analogous to that of γ'-Ni_3Al.[13] These results indicate that the LI_2 phase of γ' Ni-Si behave mechanically and structurally like γ'-Ni_3Al and therefore should produce similar strengthening effects in two phase mixtures with the respective FCC primary solid solutions.[13]

Silicon is mostly employed as an alloying element in steel, cast-iron and non-ferrous metals. In this present work the effect of silicon on precipitation kinetics in Ni-14 at. % Si alloy and variation in microhardness has been investigated.

Chapter II

Review of Literature

2.1 Properties of Pure Nickel and Silicon

The properties of pure nickel and silicon are listed in Table 2.1.1.

2.2 Phase Diagram

A complete investigation of the Ni-Si system first appeared in 1936 when Okamoto[3] studied entire composition range. However, the data as to the solubility of silicon in solid nickel were reported by various investigators.[17] The values found for room temperature by means of microscopic, X-ray and magnetic studies mainly lie close to 5 wt (~ 10 at.) % Si. At higher temperatures, however, the data points are badly scattered; in the temperature range 1100-1150°C, values between 12.7 and 17.6 at. % Si were reported.[17] The phase diagram which appeared in the Hanson and Anderko[17] is based on the results of a microscopic, X-ray, and diatometric study,[3] indicating a maximum solubility of 17.6 at. % Si at 1120°C and a solubility of 12.7 at. % Si at 900°C. This diagram is shown in Figure 2.2.1.

Klement[18] examined by means of X-ray diffraction, alloys which had been rapidly quenched from the liquid state; alloys with $\leq$15 at. % Si were single phase while an 18 at. % Si alloy yielded diffraction lines extraneous

Table 2.1.1 Properties of Pure Nickel and Silicon[15]

Property	Pure Nickel	Pure Silicon
Crystal structure	FCC	Diamond cubic
Lattice constant	3.5239 Å[16]	5.4282 Å
Density	8.902 g/cc (25°C)	2.33 g/cc (25°C)
Melting point	1453°C	1410°C
Boiling point	2730°C	2480°C
Tensile strength (annealed)	46000 psi	-
Yield strength (annealed)	8500 psi	-
Elongation (annealed)	30%	-
Compressive strength	-	13470 psi (chill cast)
Mode of rupture	-	9046 psi (chill cast)

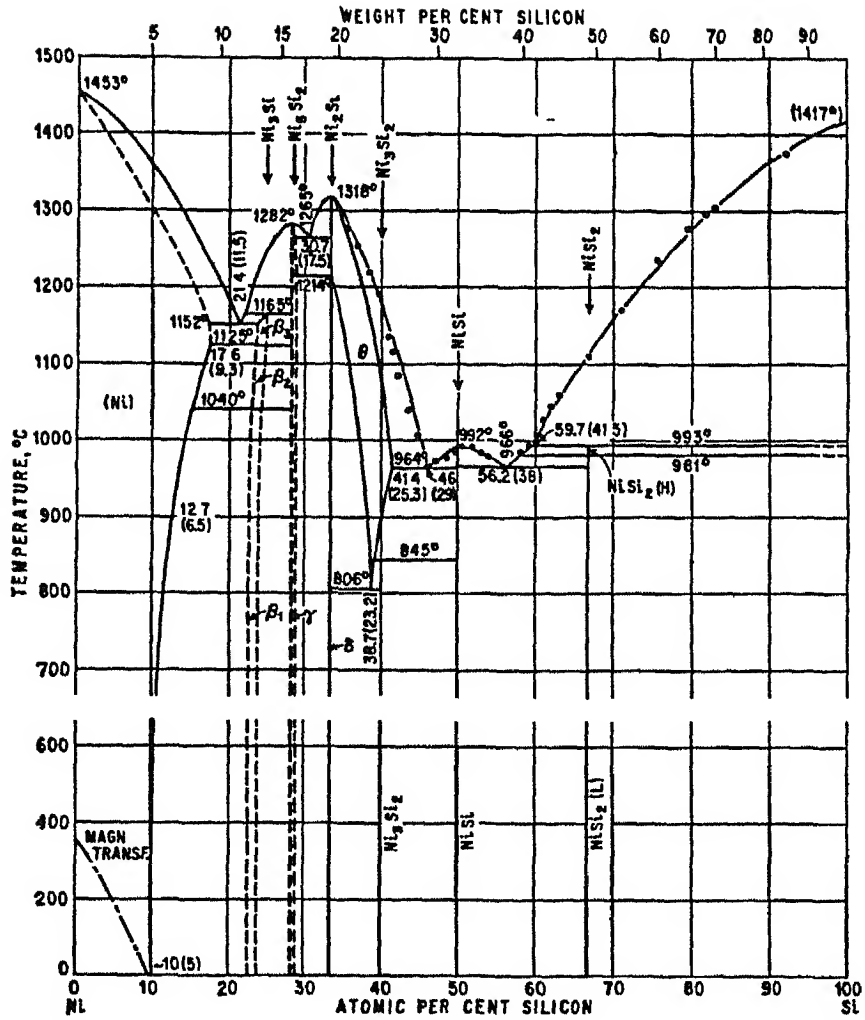

Fig. 2.2.1 : Phase diagram as appeared in Hanson and Anderko[17]

to the (Ni) pattern. These unidentified lines do not correspond to the β_1 (Ni_3Si) phase as reported by Osawa and Okamoto.[4]

Recently the Ni-rich portion of the Ni-Si phase diagram has been studied by Yoshihiro Oya and Tomoo-Suzuki.[8] According to them the solubility of silicon in FCC nickel extends to a maximum of about 15.8 at. % Si at the eutectic temperature of 1416 K (1143°C) but decreases to less than 10 at. % Si at 1000 K (727°C). This result gives a narrower solubility limit than obtained by Okamoto[3] and Klement.[18] The revised diagram which has been proposed on the basis of their work is qualitatively similar to the previous ones except as regards the mode of formation of the β-phases and the stability range of the γ-phase. The diagram is shown in Figure 2.2.2. This diagram has been examined by differential thermal analysis, X-ray diffraction and metallographic studies.

2.2.1 Crystal Structure of Intermediate Phases

An intermediate phase of the approximate composition Ni_3Si (25 at. % Si) (Ni and Si were rather impure) had already been found by Guertler and Tammann.[19] Several authors[20,21,22] assumed this phase to be stable only above 1100°C (proposed eutectoidal decomposition at about 1125°C to α and γ), but it was clearly shown by others[3,4,5,6] that Ni_3Si exists down to room temperature. According to Okamoto[3], Ni_3Si undergoes two transformations

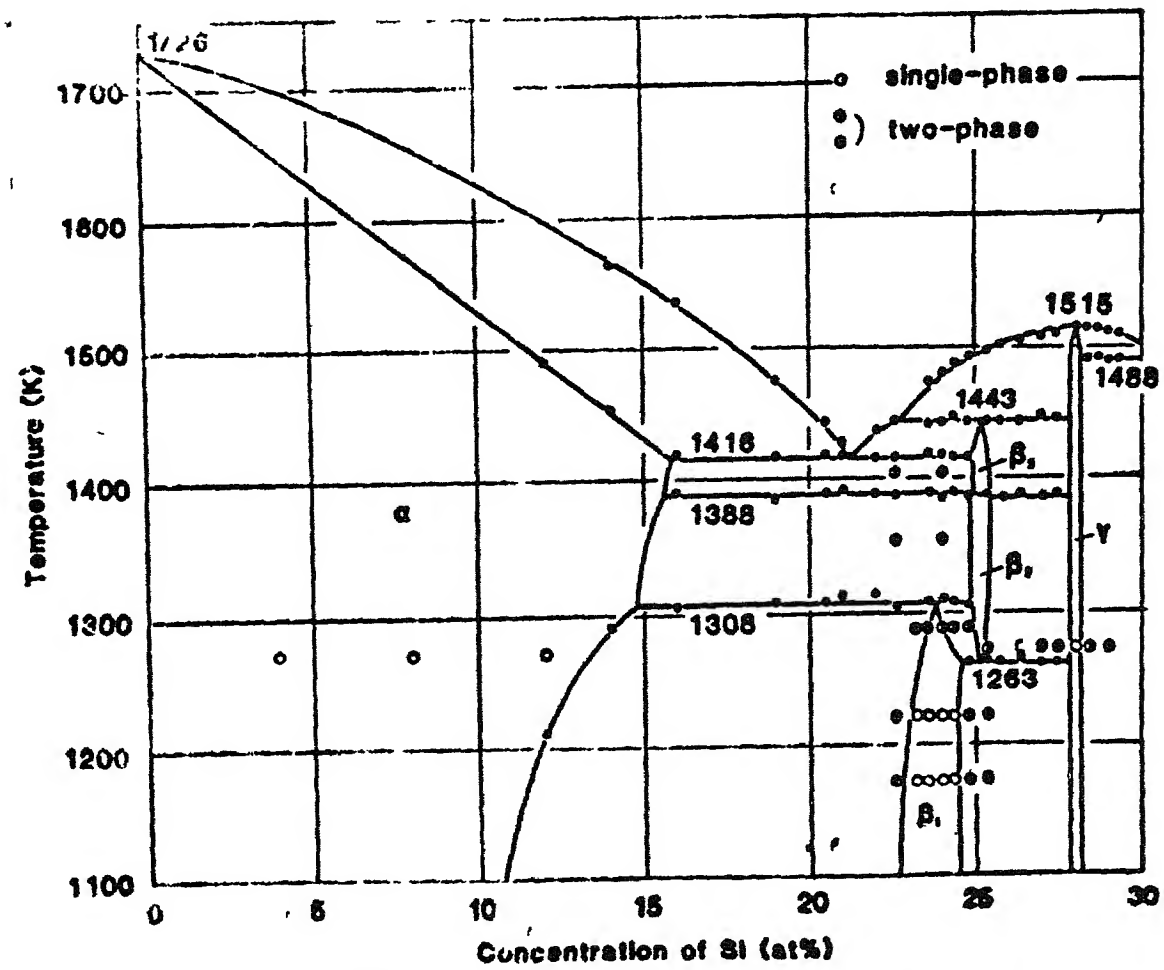

Fig.2.2.2 Nickel rich portion of the phase diagram modified by Oya and Suzuki[8]

at ~1120 and 1040°C; the three modifications are designated as β_3, β_2 and β_1 in the Figure 2.2.1. The composition of these phases alters slightly with temperature[3] resulting in eutectoid like microstructures. According to many investigators[3,4,5,6] β_1 has the cubic Cu_3Au (LI_2) type of structure, with a = 3.507 ± 5 Å.[6]

The β_3-phase formed peritectically at ~1165°C transforms to β_2 at ~1125°C, which transforms to β_1 at ~1040°C. Although the ordering transformation of β_2 to β_1 at 1040°C takes place slowly with a negligible heat effect. The changes in volume and crystal structure are clearly defined. The crystal structures of β_2-Ni_3Si and β_3-Ni_3Si has been determined by Ram and Bhan[23] by X-ray diffraction. The crystals of β_2- and β_3-Ni_3Si are pseudocubic or distorted monoclinic with a = 6.97_2 and 7.04_7, b = 6.25_4 and 6.26_4, c = 7.65_6 and 7.66_3 Å, and β = 87.75°, and 87.14°, z = 16, respectively. These phases appear to be isostructural with Pt_3Ge. The degree of monoclinic distortion depends on the atomic misfit. The structures were further confirmed by Oya and Suzuki.[8] However, Labaili and Sylavaine[24] proposed an orthorhombic (Fe_3C) structure for β_3-Ni_3Si, with lattice parameters a = 5.50, b = 6.50 and c = 4.35 Å.

Okamoto[3] describes that the stable region of the β-phases shifts slightly towards the silicon rich side with increasing temperature. The nature of this slanting of the β-phase region was conformed by Oya and Suzuki.[8] According to Lutskaya and Geld[25] the homogeneity region

of the β-phase was found to be within the limits of 22.5 and 23.4 at. % Si. But Oya and Suzuki[8] found it from 22.8 to 24.5 at. % Si, while on the other hand, both the high temperature forms β_2 and β_3 are almost stoichiometric.

In the phase diagram which has been shown in Figure 2.2.2, which was modified by Oya and Suzuki,[8] the β_1-phase forms peritectoidally at 1035°C $\alpha(Ni) + \beta_2 \rightleftarrows \beta_1$ and forms a eutectoid with the γ-phase at 990°C, $\beta_2 \rightleftarrows \beta_1 + \gamma$. The composition of the peritectoid and eutectoid reactions can be found to be 23.7 and 25.2 at. % Si respectively. The polymorphic transformation $\beta_2 \rightleftarrows \beta_3$ occurs at 1388 K, which was in good agreement with that measured by Okamoto[3] (1125°C). According to their work, the eutectic temperature $L \rightarrow \alpha + \beta_3$ is found to be 1416 K at 21.4 at. % Si while Okamoto gives 1425 K and 21.4 at. % Si, which was in good agreement.

Ni_5Si_2 (28.57 at. % Si) named γ by Iwase and Okamoto,[20] has, as Okamoto[3] showed microscopically, also a small range of homogeneity. Osawa and Okamoto[4] indexed the powder pattern tentatively with an orthohexagonal cell containing 91 atoms. Pilstrom[26] showed that the structure for Ni_5Si_2 as hexagonal (trigonal symmetry), with a parametric variation with composition, a = 6.670 A, c = 12.267 A (Si-rich) and a = 6.670 A, c = 12.332 A (Ni-rich). The trigonal symmetry of Ni_5Si_2 was further confirmed by Saini, Calvert and Taylor[27] and gave the hexagonal

parameters at stoichiometry, a = 6.68 ± 0.02 A, c = 12.28 ± 0.03 A, which is in reasonably good agreement with Pilstrom.[26]

The phase boundaries of the δ and θ phases, located at or near the composition Ni_2Si (19.31 wt. % Si) (33.34 at. %) were established by Osawa and Okamoto[4] and Iwase and Okamoto.[20] Based on the work of Osawa and Okamoto[4] on powder photographs, Toman[28] derived the structures of both δ and θ by means of measurements on monocrystals. δ or Ni_2Si (L), is orthorhombic, with a = 7.06 A, b = 4.99, c = 3.72 A, and 12 atoms per unit cell. θ, or (Ni_2Si) (H), is hexagonal, with a = 3.805 A, c = 4.890 A, c/a = 1.285 (for a 24 wt. (39.8 at.) % Si alloy quenched from 964°C), and 6 atoms per unit cell. These parameters differ only slightly from those found by Osawa and Okamoto.[4]

Ni_3Si_2 (24.19 wt. % Si) (40.01 at. % Si) is formed by a peritectoid reaction as shown by Guertler and Tammann[19] and Iwase and Okamoto.[20] The powder pattern was indexed by Osawa and Okamoto[4] with an orthohexagonal cell containing 45 atoms. Pilstrom[26] showed by single crystal and powder analysis of Ni_3Si_2 that it is orthorhombic, space group cmc2, 16 molecules per unit cell, a = 12.229 A, b = 10.805 A, c = 6.924 A.

Boren[29] reported NiSi (32.37 wt. % Si) (50.01 at. % Si) to have the cubic FeSi structure. However, Osawa and Okamoto[4] and Schubert and Pfisterer[30] showed this compound to be non-cubic, and Toman,[31] in measurements

on monocrystals, found an orthorhombic structure, with a = 5.62 A, b = 5.18 A, c = 3.34 A, and 8 atoms per unit cell. The orthorhombic MnP structure was further confirmed by Wittman et al.[32]

According to Schubert and Pfisterer[30] normal temperatures $NiSi_2$ (48.90 wt. % Si) (66.67 at. % Si) has the CaF_2 (C1) type of structure, with a = 5.406 ± 3 A. According to Osawa and Okamoto,[4] it is doubtful whether the high temperature modification of $NiSi_2$ (stable above 981°C as reported by Iwase and Okamoto,[20] while Guertler and Tammann[19] found thermal effects at about 950°C) can be quenched. Schubert and Pfisterer[30] suggested an order disorder transformation.

The results of a microscopic study of alloys with 38-98 wt. % Si as studied by Johnson and Hansen[33] are in keeping with the constitution shown in the Figure 2.2.1.

The heat of formation-composition curve showed two marked points of inflection corresponding to the compositions Ni_2Si and NiSi as reported by Oelsen and Samson.[34]

2.3 Lattice Parameters of the Solid Solutions

The nickel-silicon solid solution lattice spacings have been measured by Osawa and Okamoto[4] for alloys which are annealed at progressively lower temperatures between 1100° and 700°C and finally cooled slowly from this temperature. The measurements were obtained from back-reflection photographs taken with FeK radiation by averaging lattice

spacings from the (222) and (311) reflections. The lattice parameter versus compositions are plotted in Figure 2.3.1.

Further, Klement[18] (1962) measured the lattice parameters of Ni-Si solid solutions. Klement, using a very rapid quenching method, has extended the Ni solid solution metastably upto about 18 at. % Si. Alloys were prepared from 99.92 % Ni, 99.999% Si by melting them inductively in alumina crucibles under H_2. Compositions were estimated to $\pm$0.2 at. % from weight losses. Lattice parameters from CuK_α radiation pictures in an 11.46 cm diameter Debye-Scherrer camera. TSNR extrapolation. Temperature was 26 $\pm$ 3°C Several different determinations were made for each alloy. The lattice spacing variation shown in Figure 2.3.1, is linear with composition, the slope being $-0.5_5 \times 10^{-3}$ Å per at. % Si. The results differ from those of Osawa and Okamoto.[4] The X-ray pattern of the quenched alloy with 18 at. % Si contained a few faint extra reflections which were not due to Ni_3Si.

The lattice parameters of Ni-Si solid solutions were further determined by Oya and Suzuki[8] (1983). The solid solubility of Si in Ni was found to be decreased than earlier reported values. The modified Ni-rich portion of the phase diagram has been shown in Figure 2.2.2. The variations in lattice spacings as a function of composition are shown in Figure 2.3.1 with the data from previous investigators, Osawa and Okamoto[4] and Klement.[18]

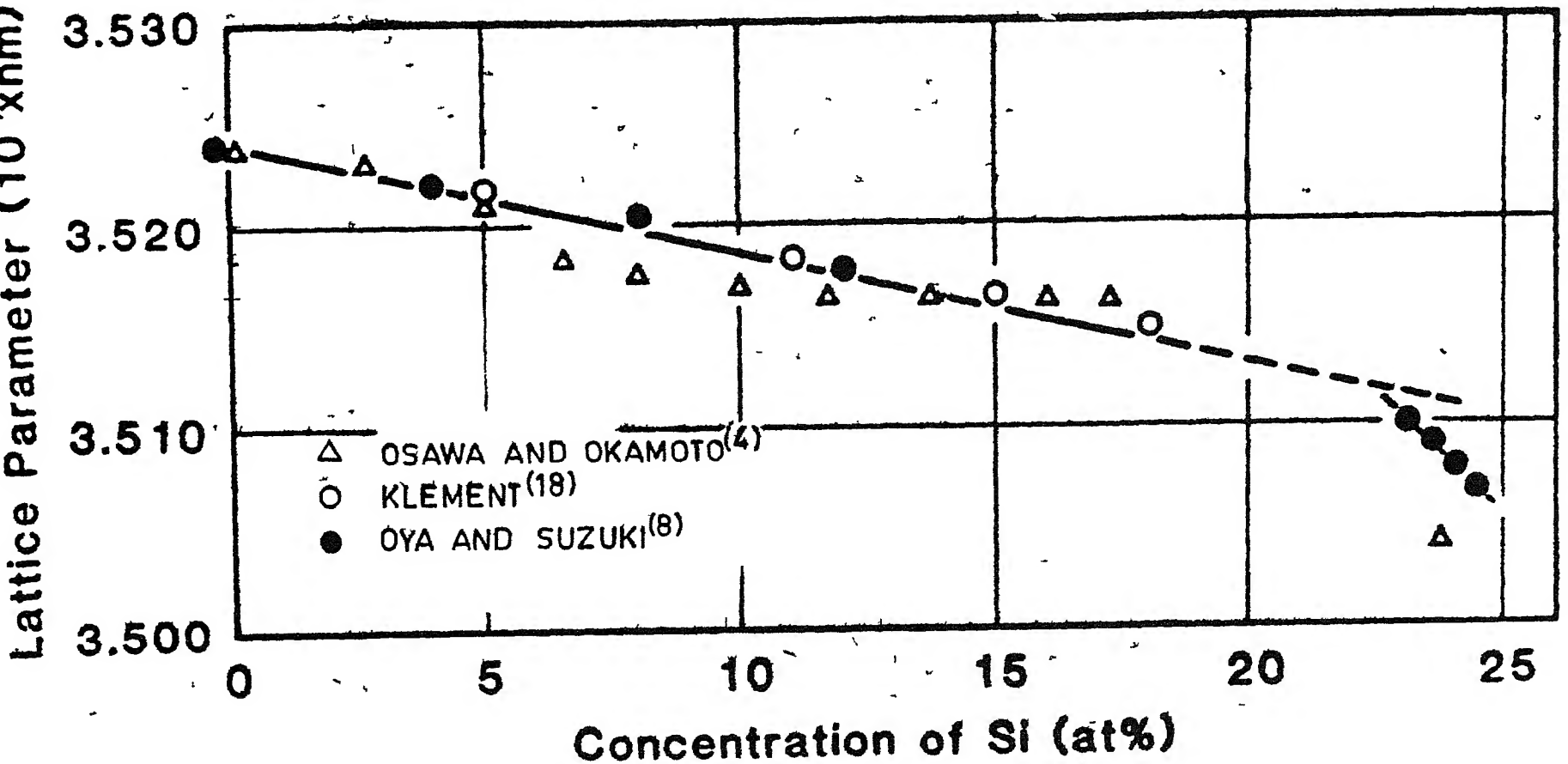

Fig.2.3.1 : Plot of lattice parameters of the solid solutions on the available data

2.4 Structure and Lattice Parameter of Ni_3Si Phase

As described earlier in the Section 2.2 that number of investigators, Okamoto,[3] Osawa and Okamoto,[4] Kusumoto[5] and Lashko[6] showed that Ni_3Si β_1 phase has the cubic Cu_3Au (LI_2) type of structure. Lutskaya and Gel'd[25] found the homogeneity range within the limits of 22.5 and 23.4 at. % Si. But Oya and Suzuki[8] (1983) found it within 22.8 and 24.5 at. % Si.

The lattice parameter of Ni_3Si β_1-phase has been given by number of investigators. Osawa and Okamoto[4] (1939) gave the lattice parameter as a = 3.496_9 KX (3.4969 x 1.00202 = 3.5031 Å) at 13.0 wt. (23.8 at. %) Si. Latter Lashko[6] (1951) studied the lattice parameter of β_1-Ni_3Si and gave the value a = 3.507 $\pm$ 5 Å. However, Badtie[35] gave the lattice parameter value a = 3.504 Å.

Recently, the lattice parameter of β_1-Ni_3Si has been studied by Labaili and Sylvaine[24] in the composition ranges of 24-26 at. % Si, and found the value a = 3.505 Å. The value is in good agreement with the published results. The lattice parameter values of β_1-Ni_3Si studied by various investigators are listed in Table 2.3.1.

2.5 Electron Microscopic and X-Ray Studies on Aged Ni-Si Alloys

It is now well established that the precipitation of γ' is a very rapid process in the binary alloys, and the growth of the γ' particles proceeds by diffusion controlled

Table 2.3.1 Lattice Parameters of β_1-Ni_3Si Phase

Compound	Space group	Lattice parameter (Å)	Composition at.%	Reference
$Ni_3Si(_1)$	$L1_2$	3.503	23.8	Osawa and Okamoto[4]
		3.507	-	Lashko[6]
		3.504	-	Badtiev[35]
		3.505	24-26	Labalii[24]

Lashko and Badtiev did not mention the compositions.

coarsening at a very early stage.[1] Chakraborty and Hornbogen[7] studied the aging characteristics of Ni-12 at. % Si and Ni-13.8 at. % Si which were solution treated for 15 hrs. at 1100°C, quenched in water and aged hardened at 600 and 750°C for periods upto 70 hrs. and examined by Transmission Electron Microscopy. It was shown that the as-quenched alloy containing Si 12 at. % has a homogeneous solid solution structure, but the alloy containing Si 13.8 at. % shows traces of Ni_3Si (γ') precipitates. On aging, the equilibrium phase Ni_3Si precipitates coherently as spheres upto 800 Å diameter and as cubes beyond this size. Discontinuous precipitation starting at grain boundaries leads to the formation of incohrent Ni_3Si. According to Labaile[24] the β_1-phase low temperature precipitate showed the sequence of cubes and then dendrites as a function of Si-supersaturation.

The process of structure formation during the slow cooling of alloys that age harden with the precipitation of the γ'-phase have been investigated by electron diffraction methods.[10] The alloy studied was Ni-6.7 wt. (13.05 at.) % Si. Rolled specimens of the alloy were homogenized at 1050°C for 1 hour and then cooled at rates of 1 and 7 °C/min to 950, 900 and 850°C and held for various times. A dendritic structure is formed in the Ni-base alloys which have different specific volumes of the matrix and the precipitated γ'-phase as well as anisotropy of the elastic properties of the matrix, during slow cooling and subsequent high temperature

aging. Dendrites are formed on faceted cubic crystals as a result of rapid tangential growth of their (100) faces, and their formation was determined by the conditions of diffusion of the dissolved atom.

During a study of Ni-Ni_5Si_2 eutectic specimens, compositions used were 7.5, 11.5, 12.1 and 16.1 wt. (14.5, 21.36, 22.35 and 28.63 at.) % Si and furnace cooled. Gardiner[36] found the another phase present in the form of very small dendrites. These microdendrites were originated from a solid state precipitation reaction. A similar morphology was also obtained for an alloy [12617-41-3] in the Ni-Ni_3Al system. The dendritic precipitate morphology is most likely to occur in systems in which the precipitating phase and matrix phase have closely similar crystal structures and similar lattice parameters.[36]

The electron microscopy and X-ray diffraction were used to study the growth, distribution and shape of γ'-precipitates and the effects thereon of dislocations in binary alloys of Ni containing Si 11.5-13.8 at. %.[10] The difference in the compound lattice parameter (ε) between precipitate particle and matrix in association with the particle size determined the distribution and shape of the precipitate viz., a homogeneous distribution of spheres, or particles (spheres or cubes) which arrange themselves in rows which subsequently coalesce to form rods. Dislocations may increase or decrease the activation energy for nucleation of γ'; at certain temperature nucleation occurs preferentially

on edge dislocations for particles with $\varepsilon \neq 0$. While at a certain degree of supersaturation particles form independently of ε in the vicinity of dislocations and in the basic lattice. Similar processes occur if γ' is metastable.

The coarsening behaviour in Ni-Si alloys has been studied in detail. Ardell[37] studied the various aspects of the Lifshitz-Wagner theory of particle coarsening using data on the γ'-precipitate in binary Ni-base alloys of Si. The kinetics of the growth of average particle, the experimental distributions of particle sizes, and the variation with time of the average solute concentration of the matrix were in excellent quantitative agreement with the predictions of the Lifshitz-Wagner theory.

Rastogi[38] studied the coarsening kinetics of Ni_3Si (γ') precipitate in a binary Ni-6.5 wt. (12.7 at.) % Si alloy by magnetic techniques and transmission electron microscopy. It was found that the variation of the silicon content of the Ni-rich matrix, as a function of time, followed Lifshitz and Wagner theory for diffusion controlled coarsening phenomenon. The established values of equilibrium solubility of Si in the matrix represent the true coherent equilibrium solubilities. The experimental particle-size distributions and average particle size were determined from dark field electron micrographs. The average particle size varied linearly with $t^{-1/3}$. The experimental distributions of particle sizes differed slightly from the theoretical curve at the early stages of aging, but the agreement

was satisfactory at the later stages. The values of the diffusion coefficient of Si, the interfacial energy, and the activation energy were calculated from the results of coarsening kinetics. The experimental value of the effective diffusion coefficient was in satisfactory agreement with the value predicted by the application of irreversible thermodynamics to the process of volume constrained growth of a coherent precipitate during coarsening. It was found that the coherent γ'-particles in Ni-Si alloy, unlike those in Ni-Al and Ni-Ti, seemed to lose coherency at high temperature. A mechanism for the formation of a semicoherent precipitate was suggested.

Rastogi[39] (1970) suggested that the loss of coherency of the γ'-phase particles on aging is due to the supply of dislocations from he Ni-matrix to the particle matrix interface by a climb process. This loss of coherency was manifested by a sudden decrease of the Si concentration in the Ni-matrix. This phenomenon appeared on aging the specimens at 775°C; it also appears at lower temperatures on specimens previously deformed by rolling.

Rastogi and Ardell[40] studied the γ'-coarsening by measuring the silicon solute kinetics. The ferromagnetic Curie temperature (°C) was determined and referred to a calibration curve of θ_c vs. solute content. The Si-concentration in the matrix of an aged 6.5 wt. (12.7 at.) % Si-alloy decreased linearly with $t^{-1/3}$ during the growth of the γ'-precipitate. The γ'-matrix interfacial free energy

obtained from the coarsening data was ~12 ergs/cm^2. The diffusion coefficient was about an order of magnitude larger than the diffusion coefficient for Si in very dilute Ni-Si alloys. The steady state distribution of particle sizes was achieved after 5 hrs. at 775°C. The γ'-particles became semicoherent after 16 hrs. aging at 775°, shown by the formation of dislocation networks at the γ'-matrix interfaces.

In a recent study Dvorack[41] studied the precipitation kinetics of the γ'-phase in a supersaturated Ni-12.5 at. % Si single crystal. It was found that the precipitation kinetics closely follows predictions of the Lifshitz and Slyozov (1961) and C. Wagner theory (1961) in both the growth and coarsening stages. The γ'-precipitate is nearly spherical during aging ≤300 hrs. at 400°C. Kinetic development of the average particle radius clearly showed a transition from first stage growth to second stage coarsening. Combining the rate constants of the 2 stages, it was possible to calculate the solute diffusivity and interphase interfacial free energy simultaneously. The method differs from that suggested by A.J. Ardell[37] in that only the particle size kinetics are needed for the current analysis, as opposed to knowledge of rate constants for both the average particle coarsening and decrease in solute concentration in the matrix.

The dissolution experiments on Ni-Si alloy system confirmed the conclusion that the solubilities of γ', determined from magnetic studies of γ'-particle coarsening, are definitely coherent solubilities.[42]

2.6 Mechanical Behaviour of Homogenised and Aged Ni-Si Solid Solutions

The mechanical properties of binary Ni-(4.1-15.6) (8.2-27.9 at.) % Si alloys were studied by Barker and Evans.[43] The alloys became progressively more brittle with increased silicon; the heat treatment of 11% Si (20.5 at.%) material at 1000°C for 16 hrs. substantially improved ductility.

The effect of solute atom on the mechanical properties of Ni was further studied by Yoshida, Takenchi and Fukuzawa.[44] The wire specimens of Ni solid solutions were strained in tension at various temperatures between liquid He and 500°K. The temperature dependence of yield stress became more pronounced with increasing solute concentration, as generally observed in FCC alloys. At high temperature, however, the yield stress decreased upto 500°K. This behaviour is different from ordinary FCC alloys. Some correlation was found between the hardening effect and the atomic size of solute element. The yield stress (σ_y) at 0°K obtained by extrapolation of the σ_y-T curve was related to the solute concentration by the equation $\sigma_y \propto c^n$, where n was a constant between 2/3 and 1. Activation volumes were determined by the strain rate change method. They turned out to be an order of magnitude larger than the value that is expected when the rate determining process is the interaction between the dislocation and each solute atom. The last two results cannot be explained by the existing theories

on solid solution hardening.

The effect of small additions of Si on the yield point of Ni has been investigated by Khayutin and Meshchaninov.[45] Stress-strain curves were determined on specimens after annealing at various temperatures. The results were interpretted in terms of Petch-Hall equation as modified by subsequent workers. It is concluded that in general alloying Ni with Si strengthens it in direct proportion to the elastic distortion although very small created in the Ni lattice by the dissolved atom. This effect is attributed to the electrochemical interaction of Si with dislocations in accordance with the Suzuki mechanism. Texture formation was found to affect the coefficient of grain boundary strengthening K_y in the Petch-Hall equation. In a marked cubic texture, K_y is less when there is elastic interaction of the additions with the grain boundaries and dislocations than it is in the absence of such a texture. This effect is in qualitative agreement with Li's theory.

The compressive flow stress of nonstoichiometric LI_2 compound Ni_3Si was measured as a function of composition at 77-800 K by Oya and Suzuki.[46] The effect of nonstoichiometry on the positively temperature dependence of strength and defect strengthening in polycrystalline Ni_3Si is similar to those found previously for Ni_3Al and Ni_3Ga alloys. The greater positive temperature dependence of strength, limited homogeneityrange within the Ni-rich side of stoichiometry, and lattice contraction in forming LI_2 ordered structure

observed in Ni_3Si and Ni_3Ge are characteristic of compounds containing 4-B subgroup elements as the minority component. The difference in extent of homogeneity range in various LI_2 compounds is explained by using an asymmetric index deduced from the free energy behaviour in the vicinity of stoichiometry. All the characteristic natures are discussed in terms of the change in bond strength.

Polycrystalline and single crystal Ni-6.5 wt. % Si (12.7 at. % Si) aged at 800°C to produce coherent particles of ordered Ni_3Si having a misfit of 0.3%, were deformed 1-2% in tension at room temperature.[47] Thin films were subsequently examined at 500 KV in an electron microscope. The deformation was inhomogeneous and caused a wide range of strains. The Orowan dislocation loops do not anneal out until temperatures are reached at which dislocation climb occurs by bulk diffusion.

The temperature dependence of the flow stress of phase Ni_3Si has been studied by Thornton and Davies.[13] Chill cast ingot of composition Ni-23.1 at. % Si was homogenized for 5 weeks at 1000°C and one week at 1050°C. The alloy was found to contain approximately 5% of second phase distributed at the grain boundaries. It was found that the degree of long range order, after quenching from 1030°C was 0.92. The result suggests that the two phase remain highly ordered upto temperatures close to limits of solubility. This behaviour is the same as that of Ni_3Al. Since an increase in the flow stress with increase in

temperature can be a consequence of a change in the degree of long range order,[48] samples were quenched from temperatures in the range 500° to 1050°C and the flow stress measured at room temperature.[13] The flow stress of quenched sample was essentially the same as that of the slowly cooled samples. This behaviour is identical to that of γ Ni_3Al, and was further confirmation of the results from X-ray studies reported above, that the alloy remain ordered at high temperatures.

The variation in flow stress with change in temperature is shown in Figure 2.6.1 for the γ'-Ni-Si phases. The flow stress increases by a factor of approximately 2 between room temperature and the peak whereas that in γ'-Ni_3Al, by a factor of approximately 5. The temperature at which the flow stress peaks occur do not appear to bear any simple relationship to the maximum temperature of stability of the phase.

An important feature of the mechanical behaviour of γ' Ni_3Al is the reversibility of the flow stress upon performing tests successively at high and low temperatures.[14] For small strains, the flow stress of γ'-Ni_3Al appears solely to be a function of the test temperature. Also γ'-Ni_3Si showed similar, reversible flow stress behaviour, entirely analogous to that of γ'-Ni_3Al.

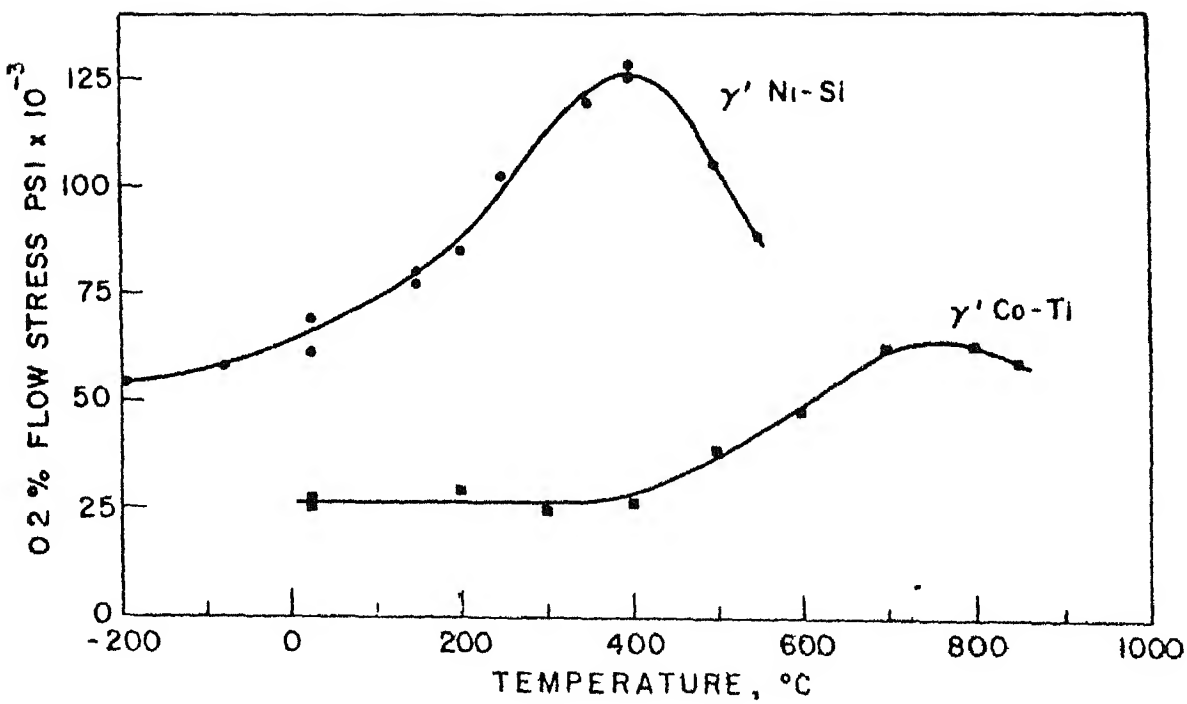

Fig.2.6.1 : Variation in flow stress with change in temperature[13]

2.6.1 Intergranular Fracture and Grain Boundary Chemistry of Ni_3Si

The intergranular fracture and grain boundary chemistry of Ni_3Si has been studied by Auger Electron Microscopy.[49] It was found that Ni_3Si is quite susceptible to grain boundary embrittlement. Ni_3Si undergoes several phase transformations between the melting point and the order-disorder transition at 1035°C. Consequently, the grain boundary facets of Ni_3Si are formed during a solid state transformation. All the Ni_3Si samples studied were found to be grain boundary brittle in both the water quenched and step cooled condition. Since sulphur segregation to grain boundaries was detected only in the step cooled samples and since in even these samples the segregation was found to be minimum for most grain boundary facets, it was concluded that the grain boundaries of Ni_3Si are intrinsically brittle.

2.6.2 Hardness during Deformation

Homogenized sheets of nickel containing 12 at. % Si were deformed by rolling at room temperature upto a 90% degree of deformation.[50] The alloys were then annealed at 600°C and changes in physical properties measured. The hardness of the moderately deformed alloys increased with annealing time, contrary to alloys deformed above 30%, which displayed practically constant hardness during annealing. Very strong deformed Ni-Si alloys showed a pronounced hardness decrease

which during annealing very little hardness change occurs is a function of alloy composition and annealing temperature employed. Electron microscopic investigations of deformed, annealed and quenched Ni-Si alloys revealed a dislocation pattern characteristic for materials of low stacking fault energy (<20 ergs/cm^2). Correspondingly treated pure Ni metal had a cell type dislocation arrangement due to a large stacking fault energy. Based on further evidence it was concluded that the decrease in hardness during annealing of increasingly deformed Ni-Si alloys is caused by preferred formation of Ni_3Si particles on dislocations, resulting in an increase of the effective average particle distance.

The experimental data were obtained concerning the hardening of binary solid solution of Ni with Si during deformation by Ageev, Guseva and Egiz.[51] By examining the elastic interaction between the screw and the edge dislocations with impurity atoms it was shown that dislocations with the predominantly edge component take part in the hardening of solid solution at the yield point. The role of the screw dislocations were not completely determined owing to the nature of the electronic interactions of the atoms in the solid solution. The deformation substructure of Ni and its solid solutions was studied by X-ray analysis. Greater disruption of the substructure, greater piling up of micro-deformations, and increase in dislocation densities were observed in the solid solutions. The dimensions of the coherent scattering regions were determined from the [111]

and [200] directions. The probability of the formation of deformation errors in the stacking was determined. The deformation substructures were included in the explanation of the deformation hardening of solid solutions. The reduction of the stacking fault energy as compared to pure Ni was found as was already reported by Chakraborty and Hornbogen.[50]

Seregin, Ivanov and Sukhovarov[52] investigated the process of structure formation in the annealing of deformed Ni that age harden with the precipitation of the γ'-phase. The alloy studied contained Ni with 6.7% (13.0 at % Si). The alloy was deformed by rolling to various degrees and annealed at various temperatures. It was found that depending on the structure of the alloys and the annealing conditions, three mechanisms operate in removing the effects of cold working and in forming a two-phase structure (1) the combined reaction of recrystallization and discontinuous decomposition; (2) the formation of a structure of the microduplex type, consisting of the grains of the γ-solid solution and γ'-phase grains; and (3) the reaction of solution of the γ'-particles at the migrating boundaries, followed by the continuous precipitation of particles within the recrystallized grains. The mechanism of the formation of the microduplex type of structure has been studied in detail. An explanation of the results obtained is advanced; in this, account is taken of the proportion by volume of the precipitated phase and the relationship between the rates of development of the processes of recrystallization and precipitation of γ'-particles in the deformed alloys.

Berezina et al.[53] studied the hardness recovery in Ni-Si alloys. It was found that in alloys with a modulated structure, hardness recovery was greatly influenced by dissolution of coherent, equilibrium, or intermediate phase precipitations providing the heat treatment was carried out above the solubility temperature for coherent precipitation. The degree of hardness recovery primarily depend on the magnitude of solid solution depletion following low-temperature aging and also on the level of coherent stresses. An explanation of this recovery is now advanced, which is based on concepts of the nonstationary stage of coalescence during two stage heat-treatment.[54] It is concluded that to explain the structure and properties of alloys containing coherent particles of precipitate under conditions of multistage heat treatment, it is necessary to take into account the position of the coherent solubility curve, the size distribution of the particles, the position of the solubility curves of the particles of the precipitated phase at the treatment temperature and the kinetics of the solution and growth of the particles at the high temperature stage of treatment.

2.7 Chemical Properties of Ni-Si Solid Solutions

2.7.1 Corrosion Resistance

The corrosion-resistance of Ni-Si alloys in acidic and alkali mediums was measured by number of investigators.

2.7.1.1 Corrosion Resistance in Acidic Medium

The addition of Si to Ni increases the resistance to H_2SO_4.[55] Further studies on corrosion resistance in H_2SO_4 solution were made on binary Ni-(4.1-15.6) % Si alloys. It was found that with cast binary alloys corrosion resistance improved progressively with Si upto 15%; the resistance showed a minimum at 7-8% Si.[43] The alloys became progressively more brittle with increased silicon; the heat treatment of 11% Si material at 1000°C for 16 hrs. substantially improved ductility and corrosion resistance in both concentrated and dilute acids.

The intergranular corrosion of nickel containing $\leq$4% silicon was studied by SEM.[56] The attack is made by potentiostatic application in an aquous H_2SO_4 solution. The close parallelism between the attack and the energy of the grain boundaries suggests a segregation of Si in the intergranular zones.

Further Beaunier et al[57] studied the general and intergranular corrosion of Ni-Si alloys containing $\leq$4% Si, cold rolled and heat treated at different times and temperatures. General and intergranular corrosion greatly increased for times <16 hrs. and low heat treatment temperatures. Long time susceptibility to intergranular corrosion did not vary. A decrease in intergranular corrosion with heat treatment time and increasing Si content was found. This effect is due to recovery and recrystallization. An effect of Si segregation in grain boundaries was additional. Short heat

treatment time results are different if the grain boundaries are parallel or perpendicular to the rolling direction.

Recently the influence of microstructure on the corrosion behaviour was studied by Kumar.[58] The Ni-base Hastelloy D [12605-86-6] containing 9% Si, 3% Cu shows high corrosion resistance to H_2SO_4, oleum and sulphate-ion environments. This alloy is characterised by the presence of intermetallic Ni_3Si-β-phase and Ni_5Si_2 γ-phase in Ni-Si solid solution as α-phase matrix. The corrosion resistance is provided by the coarse intermetallic phases. Size of intermetallic phases is dependent on the processing condition and heat treatment. The corrosion resistance can be changed by heat treatment of cast or wrought alloy. The α-phase is susceptible to corrosion more than other phases.

The intergranular corrosion studied by electron energy loss spectroscopy at high voltage and X-ray analysis showed that small silicon additions to Ni increased the intergranular corrosion with a maximum at 0.64% Si.[59] This was interpreted on the basis of segregation phenomena. Special grain boundaries with high defect density confirmed the strong segregation of Si at the boundary. Corrosion experiments were conducted with thin rolled foils containing Ni 99.36, Si 0.64 for 30 days at 1200°C in a sulphur solution. In a recent study by Lorang et al[60] also showed that small quantities of silicon improve the intergranular corrosion resistance of Ni in H_2SO_4, except for dilute alloys (0-2 at. % Si) where the increasing corrosion is attributed to Si segregation.

2.7.1.2 Hot Corrosion Study

Ni alloys containing 10.03 wt. % Si were oxidized and hot corroded in pure oxygen at 1000°C.[61] Small amounts of Si increased the oxidation rates in comparison to pure Ni in accord with the parabolic oxidation theory of the C. Wagner (1965). At high Si concentrations the oxidation rates decreased owing to the formation of oxide phases in the scale other than nickel oxide. In general, the high Si alloys showed excellent resistance to the hot corrosion process, gaining or losing <0.5 mg/cm^2 in 30 hrs. Microprobe and X-ray diffraction studies indicated that amorphous SiO_2 formed to aid in retarding both the oxidation and hot corrosion processes.

2.7.1.3 Corrosion Resistance in Alkali Medium

A study was made of the effect of addition of Si 0.36, 1.24, 1.94, 3.19% on the corrosion resistance of Ni in 65% NaOH at 180-200°C in 900 hrs. tests.[62] Specimens for corrosion testing were cut from welded joints. With increasing alloying content the corrosion rate increased, but only insignificantly compared with that of NP-2Ni. Rates were maximum after 150-250 hrs. testing and then fell with time so that at 900 hrs. all the alloys had a corrosion rate of 0.01-0.03 mm/year (NP-2Ni 0.01 mm/year). Metallographic analysis showed no intercrystalline corrosion in any case.

It was found that addition of Si $\leq$1% has practically no effect on the corrosion rate of Ni and its alloys in KOH melts.[63]

2.8 Scope of Present Work

The binary Ni-Si alloys are an important class of materials. The binary Ni-Si alloys can be hardened by coherent precipitation of the γ'-phase. Moreover, among the nickel base binary alloys, Ni-Si alloys have the smallest mismatch between the lattice spacing of precipitate and matrix so that the resulting coherency stresses around the particles are comparatively small. γ' Ni-Si also shows the reversible flow stress behaviour, entirely analogous to that of γ'-Ni_3Al. The results indicate that the γ' Ni-Si should produce strengthening effects in two phase mixtures like Ni_3Al.

In the extensive literature survey, it was found that no one has worked on the kinetics of precipitation behaviour in the Ni-Si binary alloys. In fact Ardell[40] studied the kinetics of precipitation behaviour by measuring the Curie point, but in this study, the precipitation kinetics has been studied by measuring the change in lattice parameters of supersaturated solid solution as a function of aging time, at various temperatures.

The literature survey also shows that no one has worked on the hardness of aged specimens as a function of aging temperature and time. In this work, the microhardness values of aged samples as a function of time at different temperatures has been carried out.

Chapter III

Experimental Work

3.1 Preparation of Ni-14 Atomic % Si Alloy

Pure nickel (99.999% Ni) and silicon (99.99% Si) were used for preparing the alloy. Both the pure elements were cut into pieces, weighed and mixed in required proportion (18.55389 gms. pure Ni, and 1.44625 gms. of pure Si in 20.00014 gms. of alloy) to get 14 at. % Si concentration. The samples were melted in argon atmosphere in a water cooled copper crucible using tungsten rod as non-consumable electrode. The ingot weighing 20 gms. was turned over and remelted. This operation was carried out three times. The alloy was weighed once again and no change in weight was found.

3.2 Homogenization

After removing the oxide layer on the button, the alloy was sealed under vacuum (10^{-3} mm)in quartz tube and homogenised for 24 hrs. at 1100°C. The metallography and microhardness measurements of the sample suggested that 24 hrs. time was adequate to produce homogenization.

3.3 Equipments for Heat Treatment

Homogenisation was carried out in a SiC furnace which is capable of going up to 1200°C. The hot zone of the furnace was about 6 cm in diameter and about 30 cm in depth. The temperature of the furnace was measured by Pt, Pt-13% Rh

thermocouple using an electronic milivoltmeter. The thermocouple was directly put in the furnace.

The aging of the samples was carried out in a Kanthal wound tube furnace, about 6 cm diameter. It has a central uniform hot zone where the sample was kept. The temperature was measured by Pt, Pt-13% Rh thermocouple using an electronic milivoltmeter. At the aging temperature, the temperature remained constant within $\pm 1^{\circ}C$.

The vacuum sealing was performed using a Hind Hivac vacuum system which gave a vacuum of 10^{-3} mm.

3.4 X-Ray Diffraction

X-ray diffraction was carried out on the alloy powders for the determination of lattice parameter of the alloy, change of lattice parameter of the matrix phase with aging time at different temperatures and the lattice parameter of Ni_3Si phase.

3.4.1 Preparation of Powdered Samples for X-ray Diffraction

The powders were obtained on filing the homogenised alloy. Fine powders were obtained by taking suitable precautions while filing. These powdered samples were sealed under vacuum in quartz tube, strain relieved at 1050-1100°C for 15-20 minutes, quenched in H_2O from this temperature; and aged at five different temperatures for various timings and quenched to water.

3.4.2 X-Ray Diffraction Conditions

3.4.2.1 Selection of Target Material

It is well known that, if one uses a target material with smaller characteristic radiation wavelength (K_α), the peaks will be shifted to lower angles. Hence there will be more number of peaks in the diffractograph. The more the number of peaks, the more the number of points in Nelson-Riley plot. Out of the two target materials Cu and Cr available in X-ray lab, Cu is preferred. Nickel filter is employed to suppress the background radiation and to make the incident beam as monochromatic as possible.

3.4.2.2 Range of '2θ' Used for Scanning

Initially, the diffraction patterns of all samples were taken over the entire range of 2θ (2θ = 20° to 151°) using Cu target with Ni filter. Later on, the samples were scanned over small predetermined regions where there is a probability of having peak, under certain conditions of diffractometer so as to give maximum detectability of the peaks.

3.4.2.3 Diffractometer Conditions

The diffractometer conditions for best resolution of peaks are listed below:

Radiation used	:	CuK_α
Filter used	:	Ni
Beam slit	:	2 mm

Receiving slit	:	0.3 mm
TC	:	3
Voltage	:	30 KV
Current	:	20 mA

However, the other parameters such as scanning speed, chart speed and the counts per second were changed depending on the diffraction angle and the intensity of peaks to achieve peaks with best resolution coupled with good intensity. The typical ranges of the above parameters are listed below

Scanning speed (2θ)	:	0.30°/min - 3°/min
Chart speed	:	15 mm - 30 mm
Counts per second	:	500 - 5 K

3.5 Determination of Lattice Parameter of the Homogenized and Aged Samples

The diffractographs were taken from the solution treated sample in the two phase region and of the aged samples at 5 different temperatures for various times under the above optimum conditions of diffractometer. A very precise measurement of diffraction angles (2θ) were made. Each time the diffractometer pattern of pure Ni powder (strain relieved at 700°C for 2 hrs.) was also taken, and the difference between calculated peak positions of pure Ni and measured peak positions of pure Ni was made at corresponding 2θ angles. The corresponding errors at the peak positions of sample were taken into account.

Using Bragg's law, the 'a' values are determined for all (hkl) planes for each alloy.

According to Bragg's law,

$$\lambda = 2d \sin\theta \qquad (1)$$

where λ = wavelength of the radiation used

d = interplaner spacing

θ = angle of incidence.

The alloy is FCC. For a cubic material

$$\frac{1}{d^2} = \frac{h^2 + k^2 + l^2}{a^2} \qquad (2)$$

where 'a' is the lattice parameter and (hkl) are the indices of the plane of reflection. Hence

$$a = \frac{\lambda(h^2 + k^2 + l^2)^{1/2}}{2 \sin\theta} \qquad (3)$$

The copper radiation is used for the determination of lattice parameters. λ values for Cu are as follows[64]:

$$\lambda_{CuK_\alpha} = 1.54178 \text{ Å}$$

$$\lambda_{CuK_{\alpha_1}} = 1.54051 \text{ Å}$$

$$\lambda_{CuK_{\alpha_2}} = 1.54433 \text{ Å}$$

For FCC structures, h, k and l should be unmixed. Therefore, only reflections will occur for planes (111), (200), (220), (311), (222), (400), (331), (420) etc. Since 'θ' is read from the diffraction pattern, 'a' values are determined for all (hkl) planes for each alloy. From

Nelson-Riley extrapolation method, the precise values of lattice parameters for all the samples, homogenised and aged, were determined. All the measurements were made in the laboratory where the temperature was 21 ± 1°C.

3.6 Microscopy

The samples were metallographically polished and etched. The etching agent employed was the mixture of concentrated nitric acid (50 ml), glacial acetic acid (25 ml) and water (25 ml). The microstructures were observed with optical and scanning electron microscopes.

3.7 Microhardness Measurements

The samples are polished, etched to reveal the structure. The microhardness values of the samples were determined by Leitz microhardness tester. A load of 25 P and a square-based Diamond Pyramid indentor were employed for indentation of the samples. Several indentations were made on the specimens and their average of microhardness values were taken.

Chapter IV

Results

4.1 Homogenized Sample

The cast alloy containing 14 at. % Si in nickel homogenized in vacuum sealed quartz tube at 1100°C for 24 hrs. and quenched in water showed homogenised microstructure shown in Figure 4.1.1. The microhardness of this sample was measured, the values are tabulated in Table 4.1.1.

The microhardness of another sample treated in a similar manner but aircooled from homogenisation temperature was also measured, the values are shown in Table 4.1.1.

In order to measure the lattice parameter of this alloy, powders of the homogenised sample were taken, they were vacuum sealed and annealed at 1050°C for 20 minutes and water quenched. These strain relieved powders are used for X-ray measurements along with pure nickel powders which were used as standard whose lattice parameter has earlier been determined using a quartz standard as 3.5239 Å.

The angular position of peaks from the nickel powders as well as the Ni-14 at. % Si alloys are listed in Table 4.1.2. The Table 4.1.2 also lists the theoretical positions of pure nickel, the error in these peaks and the corrected values of the peak positions of Ni-14 at. % Si alloy. From these data, the 'a' values and the Nelson-Riley function have been calculated and listed in the Table 4.1.2.

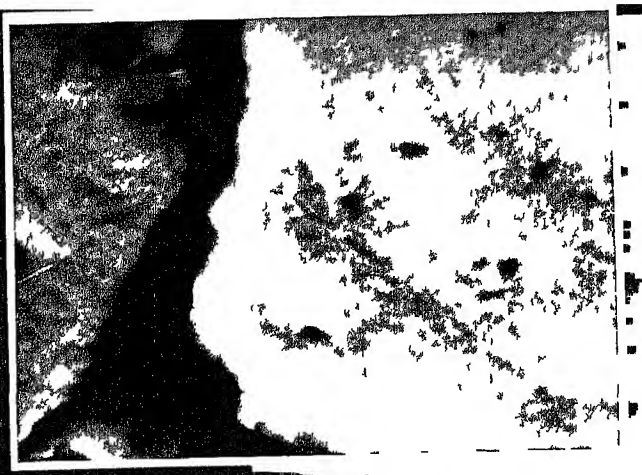

Fig. 4.1.1(e)

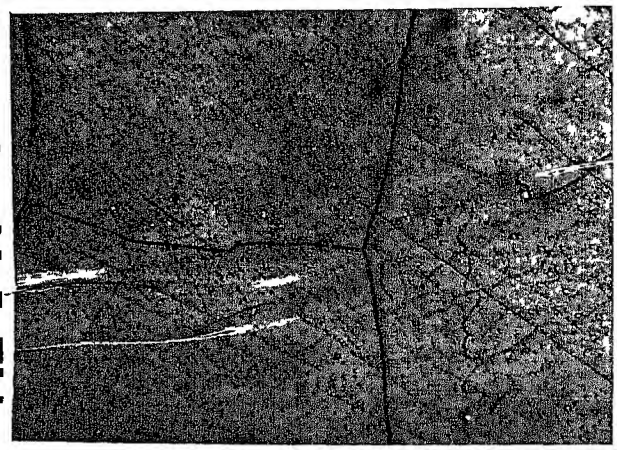

Fig. 4.1.1(f)

Fig. 4.1.1(g)

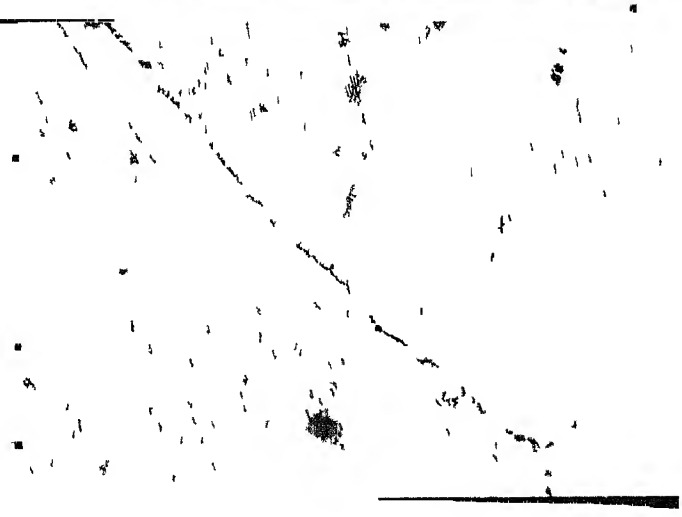

Fig. 4.1.1(h)

Fig. 4.1.1 (continued)

(e) Sample aircooled from homogenisation temperature and aged at 700°C for 40 hrs., 7000X

(f) Sample quenched from homogenisation temperature and aged at 650°C for 7 hrs., 1000X

(g) Sample quenched from homogenisation temperature and aged at 650°C for 22 hrs., 750X

(h) Sample aircooled from homogenisation temperature and aged at 750°C for 241 hrs., 3000X

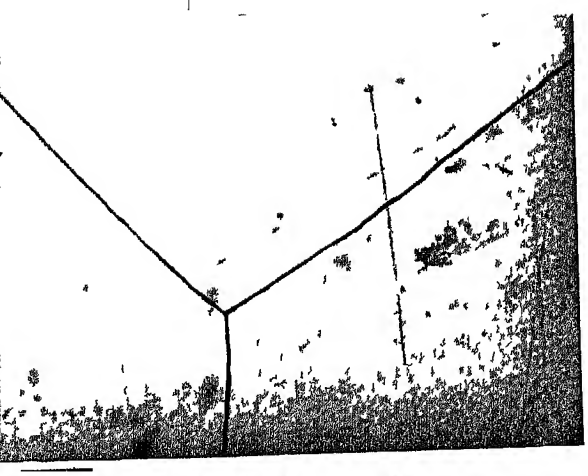

Fig. 4.1.1(a)

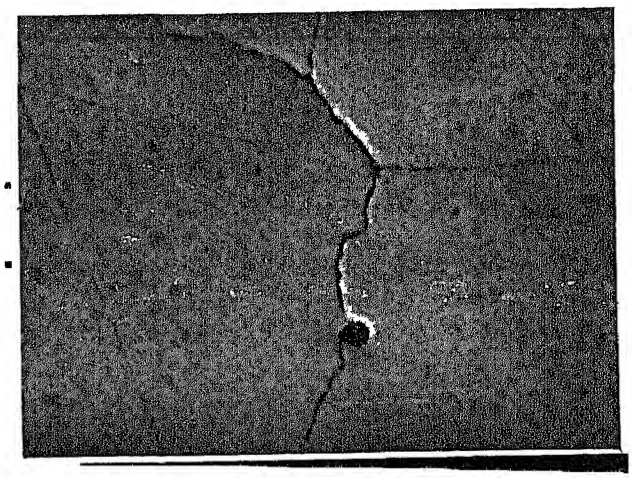

Fig. 4.1.1(b)

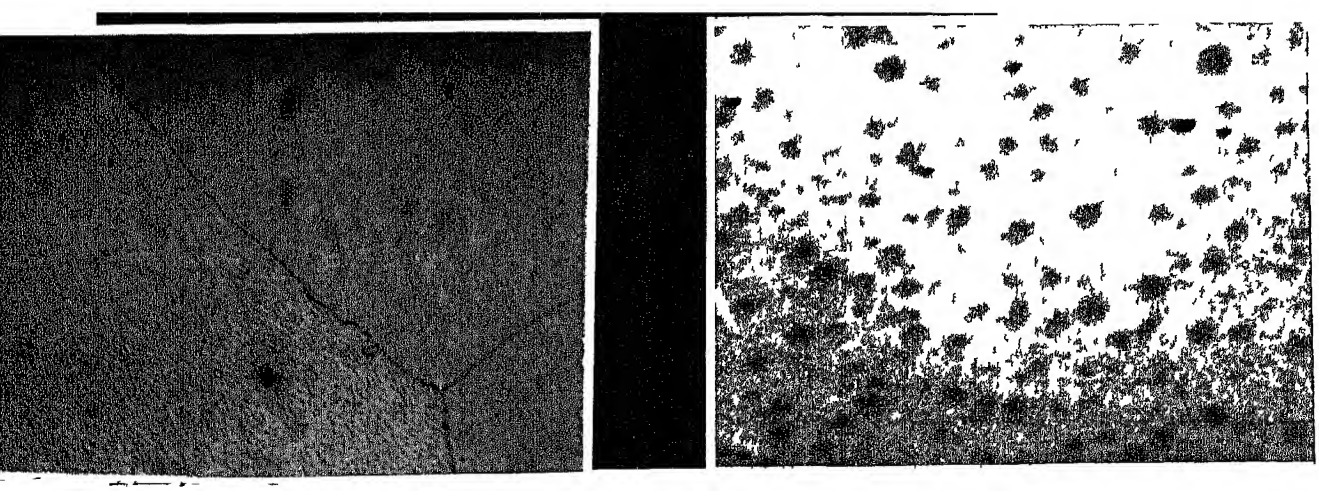

Fig. 4.1.1(d)

Fig. 4.1.1 Microstructures of homogenised and aged alloys
(a) Sample homogenised at 1100°C for 24 hrs. and quenched in H_2O, 500X
(b) Sample aircooled from homogenisation temperature and aged at 750°C for 70 hrs., 500X
(c) Sample aircooled from homogenisation temperature and aged at 750°C for 70 hrs., 1000X
(d) Sample aircooled from homogenisation temperature and aged at 750°C for 241 hrs., 500X

Table 4.1.1 Microhardness Values of Ni-14 at. % Si Alloy, Homogenized and Aged Samples

Treatment	Temperature	Time	Microhardness (DPN)
(a) Homogenized and quenched	1100°C	24 hrs.	503
Aged at	650°C	1 hr.	552
		4 hrs.	589
		7 hrs.	563
(b) Homogenized and aircooled	1100°C	24 hrs.	440
Aged at	750°C	1 hr.	419
		2 hrs.	410
		6 hrs.	413
		10 hrs.	402
		70 hrs	399
		150 hrs.	398
		241 hrs.	398
	700°C	1 hr.	486
		2 hrs.	456
		3 hrs.	446
		4 hrs.	449
		5 hrs.	444
		10 hrs.	444
		40 hrs.	411

Table 4.1.2 Calculation of 'a' Values from Diffraction Pattern of Homogenized and Quenched Ni-14 at. % Si Alloy, Strain Relieved at 1050°C for 20 minutes

Reflecting plane	Pure nickel			Ni-14 at. % Si alloy homogenized at 1050°C for 20 minutes				
	Theoretical 2θ	Measured 2θ	Error 2θ	Measured 2θ	Corrected error 2θ	Corrected	'a' in nm	$\frac{\cos^2\theta}{\sin\theta} + \frac{\cos^2\theta}{\theta}$
$(220)_{\alpha_1}$	76.37521	76.29	-0.08521	76.49875	-0.08514	76.58389	0.351577	1.91580
$(220)_{\alpha_2}$	76.59888	76.5137	-0.08513	76.6925	-0.08517	76.77777	0.351696	1.90627
$(311)_{\alpha_1}$	92.92917	92.8375	-0.09167	93.1025	-0.09455	93.19705	0.351610	1.23030
$(311)_{\alpha_2}$	93.22864	93.1337	-0.09489	93.36125	-0.09526	93.45651	0.351730	1.221418
$(222)_{\alpha_1}$	98.43319	98.33	-0.10319	98.60625	-0.10105	98.70730	0.351665	1.05181
$(222)_{\alpha_2}$	98.76312	98.6625	-0.10062	98.92	-0.10034	99.02034	0.351714	1.04227
$(331)_{\alpha_1}$	144.6407	144.5975	-0.04320	145.185	-0.05488	145.23988	0.351808	0.16390

The 'a' values are plotted against the Nelson-Riley function in Figure 4.1.2. The best straight line through the experimental points gives the value of 'a' as 0.351810 nm.

4.2 Effect of Aging

4.2.1 Aging Temperature at 850°C

Powders of the homogenised alloys quenched from 1050°C, were aged for 20 hrs. and 38 hrs. and their X-rays were taken with nickel standard. These X-ray data were analysed in a manner described above. The raw data for 20 hrs. of aging is given in Table 4.2.1 and the corresponding plot is in Figure 4.2.1. The raw data for 38 hrs. of aging is in Table 4.2.2 and the Nelson-Riley plot is in Figure 4.2.1. The 'a' values are listed in Table 4.1.3. The lattice parameters are plotted against aging time in Figure 4.2.2.

4.2.2 Aging Temperature at 750°C

The powders of sample quenched from 1050°C for 20 minutes are aged at 1, 2, 10, 150 and 310 hrs. and examined by X-ray. The raw data are given in Tables 4.2.3, 4.2.4, 4.2.5, 4.2.6 and 4.2.7. The Nelson-Riley plots are given in Figure 4.2.3. The 'a' values are listed in Table 4.1.3 and are plotted as a function of aging time in Figure 4.2.2.

Bulk samples of the alloy were aircooled from homogenised temperature and aged at 750°C for various lengths of time. The microhardness values are listed in Table 4.1.1. They are also plotted in Figure 4.1.3.

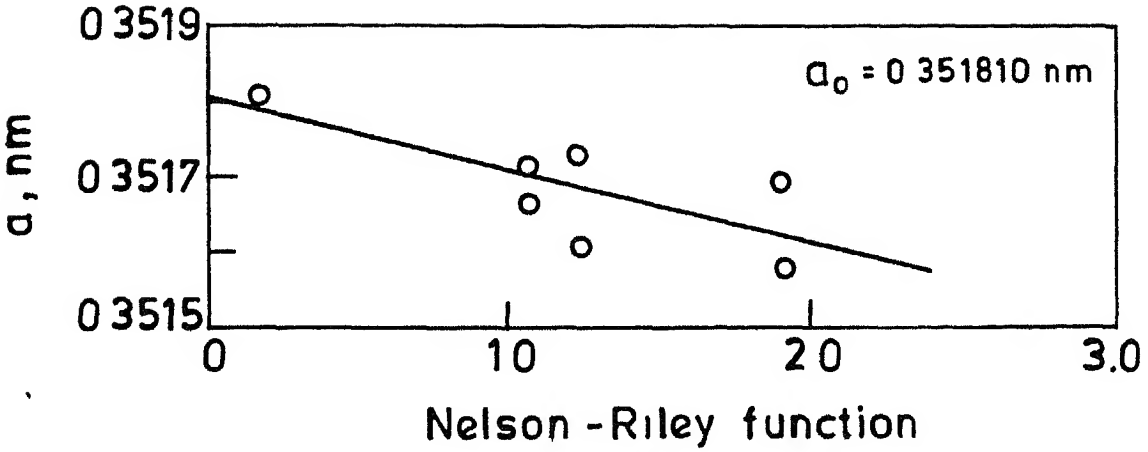

Fig 4.1 2 Nelson - Riley plot for sample homogenised, strain relieved and quenched.

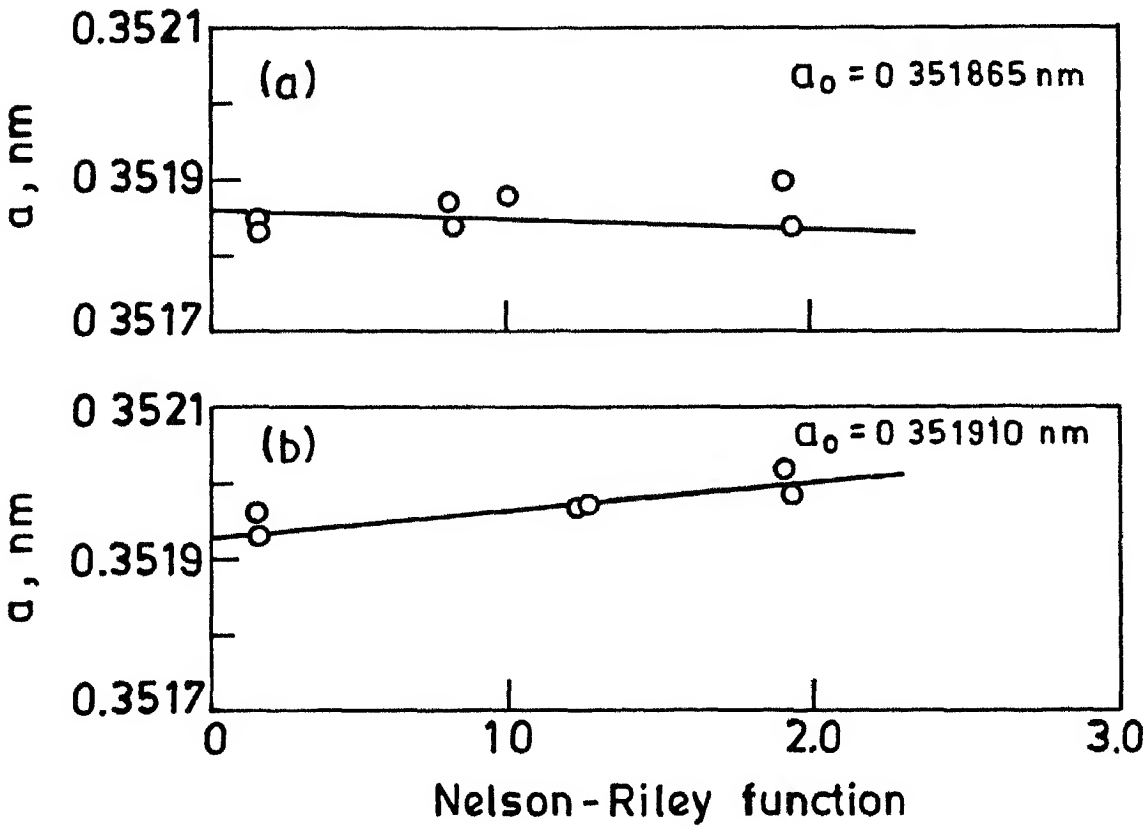

Fig 4.2.1 Nelson - Riley plots for sample aged at 850°C for (a) 20 hrs (b) 38 hrs

The structures of the samples aged at 750°C for various times are shown in Figure 4.1.1.

4.2.3 Aging Temperature at 700°C

Quenched powders from the homogenised temperature were aged at 700°C for 1, 2, 4, 10 and 40 hrs. of time and their X-ray diffraction pattern were taken using nickel as standard. The raw data are listed in Tables 4.2.8, 4.2.9, 4.2.10, 4.2.11 and 4.2.12 and Nelson-Riley functions are plotted in Figure 4.2.4. The 'a' values are listed in Table 4.1.3 and are plotted against aging time in Figure 4.2.2.

The bulk samples aircooled from homogeneous temperature were aged and microhardness values are measured. They are listed in Table 4.1.1 and plotted against aging time in Figure 4.1.3.

The structure of bulk samples aircooled from homogeneous temperature and aged at 700°C for 10 hrs. is shown in Figure 4.1.1.

4.2.4 Aging Temperature at 650°C

Powder samples quenched and aged at 650°C were subjected to X-ray measurements. The data are given in Tables 4.2.13, 4.2.14 and 4.2.15 and Nelson-Riley functions are plotted in Figure 4.2.5. The 'a' values are listed in Table 4.1.3 and these are plotted against aging time in Figure 4.2.2.

The microhardness values of bulk samples quenched from homogenisation temperature and aged at 650°C have been measured. They are listed in Table 4.1.1 and are plotted against aging time in Figure 4.1.3.

The microstructure of sample aged upto 7 hrs. are shown in Figure 4.1.1.

4.2.5 Aging Temperature at 600°C

Powder samples quenched from homogenisation temperature were aged at 600°C and their diffraction pattern were taken. The data are listed in Table 4.2.16 and Table 4.2.17 and the Nelson-Riley plots are in Figure 4.2.6. The 'a' values are listed in Table 4.1.3 and are plotted as a function of aging time in Figure 4.2.2.

Table 4.1.3 Lattice Parameters of Homogenized and Matrix Phase of Aged Samples

Treatment	Temperature (°C)	Time (hrs.)	Lattice parameter (nm)
Homogenized and quenched	1100	24	
Strain relieved	1050	0.33	0.351810
Powders quenched from homogenized temperature and aged at	850	20	0.351865
		38	0.351910
	750	1	0.351890
		2	0.351910
		10	0.351946
		150	0.351975
		310	0.351975
	700	1	0.351872
		2	0.351911
		4	0.351940
		10	0.352003
		40	0.352022
	650	92	0.351860
		165	0.351887
		198	0.351939
	600	22	0.351812
		85	0.351832

Table 4.2.1 Calculation of 'a' Values for the Matrix Phase from Diffraction Pattern of Ni-14 at. % Si; Aged at 850°C for 20 hrs.

Reflecting plane	Pure nickel			Ni-14 at. % Si alloy, aged at 850°C for 20 hrs.					Additional peaks corrected 2θ
	Theoretical 2θ	Measured 2θ	Error 2θ	Measured 2θ	Corrected error 2θ	Corrected 2θ	'a' in nm	$\frac{\cos^2\theta}{\sin\theta} + \frac{\cos^2\theta}{\theta}$	
$(220)_{\alpha_1}$	76.3752	76.2713	-0.1040	76.4158	-0.1000	76.5158	0.351841	1.9192	
$(220)_{\alpha_2}$	76.5989	76.5013	-0.0976	76.6281	-0.0976	76.7257	0.351897	1.9088	
$(311)_{\alpha_1}$	92.9292	92.8388	-0.0904	93.0118	-0.0919	93.1037	0.351881	1.2335	
$(222)_{\alpha_1}$	98.4332	98.3300	-0.1039	98.5353	-0.1067	98.6420	0.351838	1.0538	
$(222)_{\alpha_2}$	98.7631	98.6544	-0.1087	98.8526	-0.1087	98.9613	0.351869	1.0431	99.2493 α_1
$(331)_{\alpha_1}$	144.6407	144.5744	-0.0663	145.1363	-0.0842	145.2205	0.351827	0.1641	
$(331)_{\alpha_2}$	145.5433	145.4491	-0.0942	146.0025	-0.1118	146.1143	0.351851	0.1554	

Table 4.2.2 Calculation of 'a' Values for the Matrix Phase from Diffraction Pattern of Ni-14 at. % Si; aged at 850°C for 38 hrs.

Reflecting plane	Pure nickel			Ni-14 at. % Si alloy, aged at 850°C for 38 hrs.					
	Theoretical 2θ	Measured 2θ	Error 2θ	Measured 2θ	Corrected error 2θ	Corrected 2θ	'a' in nm	$\frac{\cos^2\theta}{\sin\theta} + \frac{\cos^2\theta}{\theta}$	Additional peaks corrected 2θ
$(220)_{\alpha_1}$	76.3752	76.2838	-0.0914	76.3887	-0.0905	76.4792	0.351984	1.9210	76.9228_{α_1}
$(220)_{\alpha_2}$	76.5989	76.5094	-0.0895	76.6045	-0.0895	76.6940	0.352020	1.9104	
$(311)_{\alpha_1}$	92.9292	92.8452	-0.0840	92.9844	-0.0883	93.0727	0.351971	1.2346	93.6594_{α_1}
$(311)_{\alpha_2}$	93.2286	93.1356	-0.0930	93.2800	-0.0936	93.3736	0.351969	1.2243	93.9820_{α_2}
									99.2480_{α_1}
$(331)_{\alpha_1}$	144.6407	144.5714	-0.0693	145.0500	-0.0623	145.1123	0.351931	0.1652	
$(331)_{\alpha_2}$	145.5433	145.4874	-0.0559	145.9488	-0.0492	145.9979	0.351960	0.1565	

98041

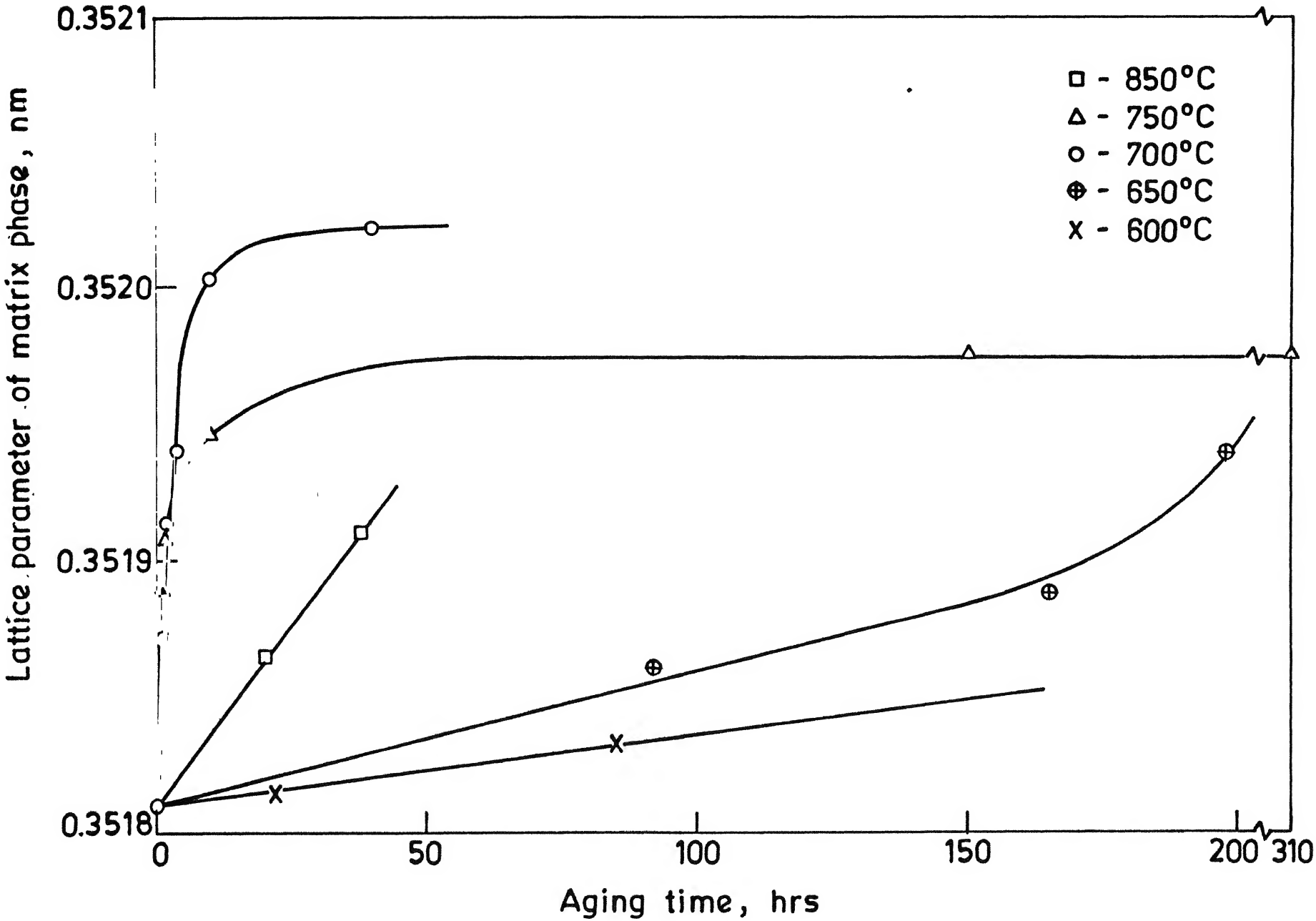

Fig 4.2.2 Plot of lattice parameter of matrix phase vs aging time at different

Table 4.2.3 Calculation of 'a' Values for the Matrix Phase from Diffraction Pattern of Ni-14 at. % Si Alloy; Aged at 750°C for 1 hr.

Reflecting plane	Pure nickel			Ni-14 at. % Si alloy, aged at 750°C for 1 hr.					
	Theoretical 2θ	Measured 2θ	Error 2θ	Measured 2θ	Corrected error 2θ	Corrected 2θ	'a' in nm	$\frac{\cos^2\theta}{\sin\theta} + \frac{\cos^2\theta}{\theta}$	Additional peaks corrected 2θ
$(220)_{\alpha_1}$	76.3752	76.2738	-0.1015	76.4100	-0.0977	76.5077	0.351871	1.9196	
$(311)_{\alpha_1}$	92.9292	92.8463	-0.0829	93.0025	-0.0826	93.0851	0.351935	1.2341	
$(222)_{\alpha_1}$	98.4332	98.3359	-0.0973	98.5025	-0.0914	98.5939	0.351965	1.0553	99.2362_{α_1}
$(331)_{\alpha_1}$	144.6407	144.5523	-0.0884	145.0574	-0.0751	145.1325	0.351912	0.1650	146.8540_{α_1}

Table 4.2.4 Calculation of 'a' Values for the Matrix Phase from Diffraction Pattern of Ni-14 at. % Si Alloy; Aged at 750°C for 2 hrs.

Reflecting plane	Pure nickel			Ni-14 at. % Si alloy, aged at 750°C for 2 hrs.					
	Theoretical 2θ	Measured 2θ	Error 2θ	Measured 2θ	Corrected error 2θ	Corrected 2θ	'a' in nm	$\frac{\cos^2\theta}{\sin\theta} + \frac{\cos^2\theta}{\theta}$	Additional peaks corrected 2θ
$(220)_{\alpha_1}$	76.3752	76.2738	-0.1015	76.4110	-0.0977	76.5087	0.351869	1.9196	
$(220)_{\alpha_2}$	76.5989	76.5038	-0.0951	76.6278	-0.0950	76.7229	0.351903	1.9090	
$(311)_{\alpha_1}$	92.9292	92.8463	-0.0829	93.0345	-0.0826	93.1171	0.351842	1.2330	
$(311)_{\alpha_1}$	93.2286	93.1463	-0.0824	93.2857	-0.0828	93.3685	0.351984	1.2244	
$(222)_{\alpha_1}$	98.4332	98.3359	-0.0973	98.5188	-0.0908	98.6096	0.351920	1.0548	99.1452_{α_1}
$(222)_{\alpha_2}$	98.7631	98.6780	-0.0851	98.8392	-0.0851	98.9243	0.351966	1.0452	99.5000_{α_2}
$(331)_{\alpha_1}$	144.6407	144.5523	-0.0884	145.1439	-0.0729	145.2168	0.351831	0.1641	146.8180_{α_1}
$(331)_{\alpha_2}$	145.5433	145.4793	-0.0640	145.9875	-0.0640	146.0515	0.351906	0.1557	

Table 4.2.5 Calculation of 'a' Values for the Matrix Phase from Diffraction Pattern of Ni-14 at. % Si; Aged at 750°C for 10 hrs.

Reflecting plane	Pure nickel			Ni-14 at. % Si alloy, aged at 750°C for 10 hrs.					
	Theoretical 2θ	Measured 2θ	Error 2θ	Measured 2θ	Corrected error 2θ	Corrected 2θ	'a' in nm	$\frac{\cos^2\theta}{\sin\theta} + \frac{\cos^2\theta}{\theta}$	Additional peaks corrected 2θ
$(220)_{\alpha_1}$	76.3752	76.2644	-0.1108	76.3442	-0.1101	76.4543	0.352081	1.9222	
$(220)_{\alpha_2}$	76.5989	76.4900	-0.1089	76.5400	-0.1088	76.6488	0.352196	1.9126	
$(311)_{\alpha_2}$	93.2286	93.1213	-0.1073	93.2413	-0.1071	93.3484	0.352042	1.2251	
$(222)_{\alpha_1}$	98.4332	98.3350	-0.0982	98.4671	-0.0933	96.5604	0.352053	1.0563	
$(222)_{\alpha_2}$	98.7631	98.6776	-0.0855	98.7860	-0.0855	98.8715	0.352105	1.0468	99.2055_{α_1}
$(331)_{\alpha_1}$	144.6407	144.5553	-0.0854	145.0123	-0.0787	145.9013	0.351952	0.1654	
$(331)_{\alpha_2}$	145.5433	145.4713	-0.0721	145.8650	-0.0721	145.9371	0.352017	0.1574	

Table 4.2.6 Calculation of 'a' Values for the Matrix Phase from Diffraction Pattern of Ni-14 at. % Si, Aged at 750°C for 150 hrs.

Reflecting plane	Pure nickel			Ni-14 at. % Si alloy, aged at 750°C for 150 hrs.					
	Theoretical 2θ	Measured 2θ	Error 2θ	Measured 2θ	Corrected error 2θ	Corrected 2θ	'a' nm	$\frac{\cos^2\theta}{\sin\theta} + \frac{\cos^2\theta}{\theta}$	Additional peaks corrected 2θ
$(220)_{\alpha_1}$	76.3752	76.2269	-0.1483	76.4000	-0.1477	76.5477	0.351717	1.9176	No extra peak could be measured accurately
$(220)_{\alpha_2}$	76.5989	76.4514	-0.1475	76.6213	-0.1474	76.7686	0.351731	1.9067	
$(311)_{\alpha_1}$	92.9292	92.7944	-0.1348	93.0062	-0.1362	93.1424	0.351769	1.2322	
$(311)_{\alpha_2}$	93.2286	93.0919	-0.1367	93.2599	-0.1371	93.3970	0.351902	1.2234	
$(222)_{\alpha_1}$	98.4332	98.2845	-0.1487	98.4975	-0.1450	98.6425	0.351836	1.0538	
$(222)_{\alpha_2}$	98.7631	98.6203	-0.1428	98.8075	-0.1428	98.9503	0.351900	1.0444	
$(331)_{\alpha_1}$	144.6407	144.5485	-0.0922	145.0238	-0.0920	145.1158	0.351930	0.1648	
$(331)_{\alpha_2}$	145.5433	145.4514	-0.0919	145.9175	-0.0919	146.0094	0.351949	0.1564	

Table 4.2.7 Calculation of 'a' Values for the Matrix Phase from Diffraction Pattern of Ni-14 at. % Si, aged at 750°C for 310 hrs.

Reflecting plane	Pure nickel			Ni-14 at. % Si alloy, aged at 750°C for 310 hrs.					
	Theoretical 2θ	Measured 2θ	Error 2θ	Measured 2θ	Corrected error 2θ	Corrected 2θ	'a' nm	$\frac{\cos^2\theta}{\sin\theta} + \frac{\cos^2\theta}{\theta}$	Additional peaks corrected 2θ
$(311)_{\alpha_1}$	92.9292	92.8063	-0.1229	92.9421	-0.1255	93.0676	0.351986	1.2347	76.957_{α_1}
$(311)_{\alpha_2}$	93.2286	93.1000	-0.1286	93.2253	-0.1285	93.3539	0.352027	1.2249	93.6424_{α_1}
$(222)_{\alpha_1}$	98.4332	98.3087	-0.1245	98.4629	-0.1208	96.5836	0.351992	1.0556	
$(222)_{\alpha_2}$	98.7631	98.6468	-0.1163	98.7960	-0.1163	98.9122	0.351998	1.0456	
$(400)_{\alpha_1}$	121.9295	121.8239	-0.1056	122.0481	-0.1074	122.1555	0.352005	0.4866	
$(400)_{\alpha_2}$	122.4434	122.3337	-0.1097	122.5565	-0.1097	122.6422	0.352015	0.4777	
$(331)_{\alpha_1}$	144.6407	144.5264	-0.1143	144.9688	-0.1052	145.0739	0.351968	0.1655	146.8454_{α_1}
$(331)_{\alpha_2}$	145.5433	145.4479	-0.0954	145.8838	-0.0954	145.9791	0.351977	0.1568	

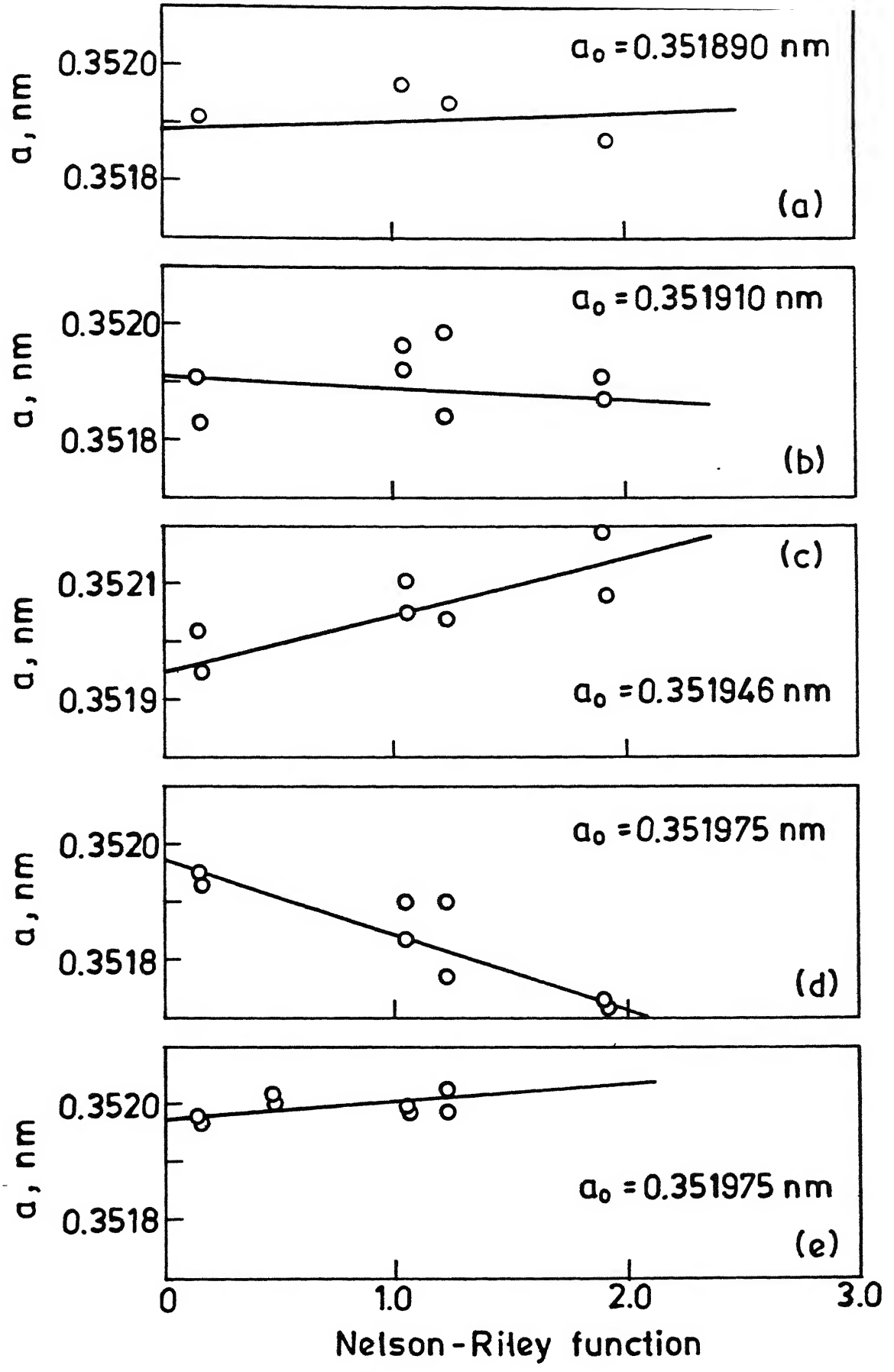

Fig. 4.2.3 Nelson-Riley plots for sample aged at 750°C for (a) 1 hr (b) 2 hrs (c) 10 hrs (d) 150 hr and (e) 310 hrs.

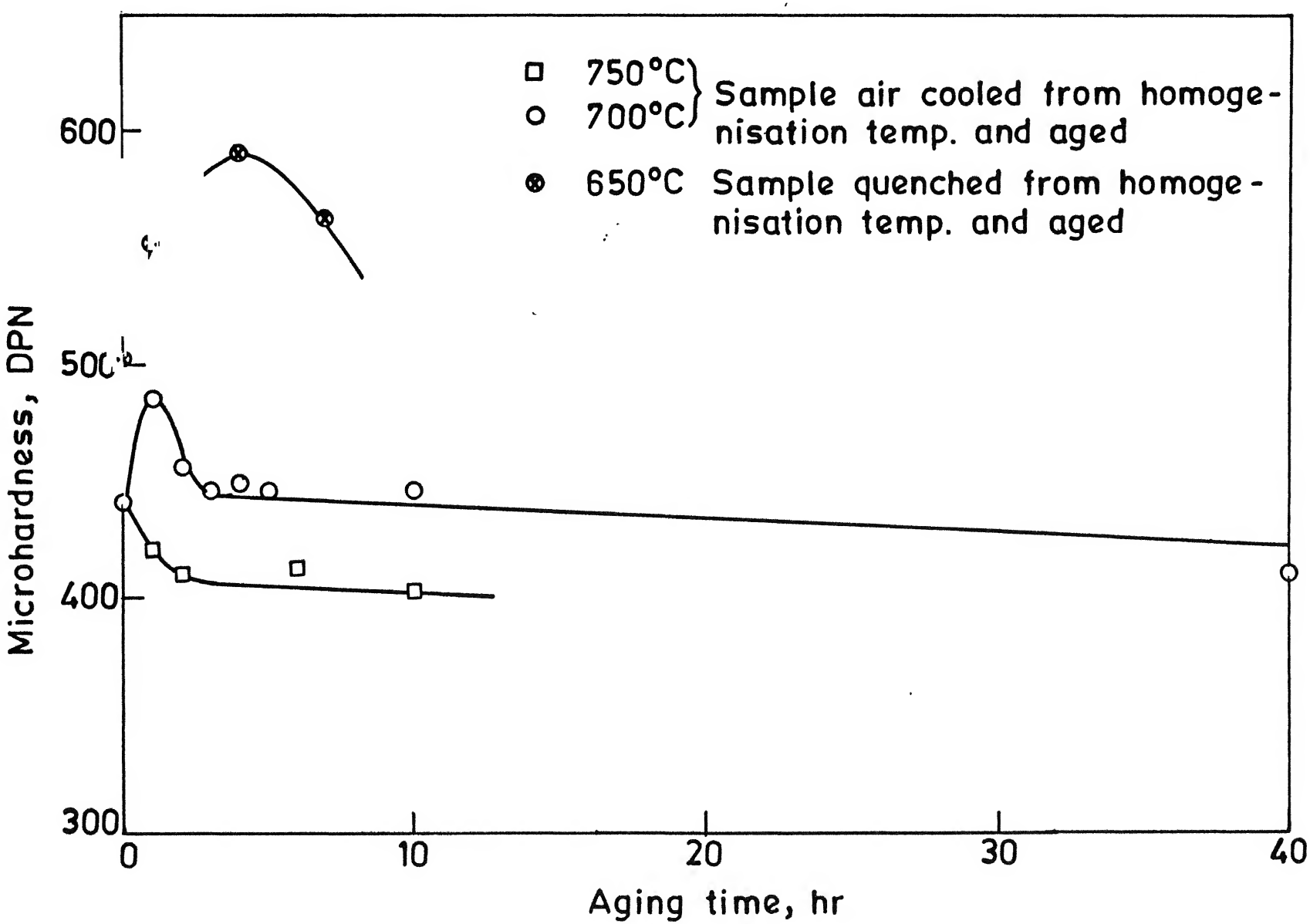

Fig. 4.1.3 Plot of microhardness vs aging time.

Table 4.2.8 Calculation of 'a' Values for the Matrix Phase from Diffraction Pattern of Ni-14 at. % Si, Aged at 700°C for 1 hr.

Reflecting plane	Pure nickel			Ni-14 at. % Si alloy, aged at 700°C for 1 hr.					
	Theoretical 2θ	Measured 2θ	Error 2θ	Measured 2θ	Corrected error 2θ	Corrected 2θ	'a' nm	$\frac{\cos^2\theta}{\sin\theta} + \frac{\cos^2\theta}{\theta}$	Additional peaks corrected 2θ
(220)	76.4495	76.3646	-0.0849	76.5650	-0.0850	76.6500	0.351610	1.9126	
(311)	93.0286	92.9363	-0.0924	93.1863	-0.0930	93.2793	0.351661	1.2275	
$(222)_{\alpha_1}$	98.4332	98.3300	-0.1032	98.5900	-0.1012	98.6912	0.351708	1.0523	Extra peaks could not be measured accurately
$(222)_{\alpha_2}$	98.7631	98.6625	-0.1006	98.8750	-0.0985	98.9735	0.351837	1.0437	
$(331)_{\alpha_1}$	144.6407	144.5975	-0.0432	145.0900	-0.0520	145.1420	0.351903	0.1649	

Table 4.2.9 Calculation of 'a' Values for the Matrix Phase from Diffraction Pattern of Ni-14 at. % Si, aged at 700°C for 2 hrs.

Reflecting plane	Pure nickel			Ni-14 at. % Si alloy, aged at 700°C for 2 hrs.					
	Theoretical 2θ	Measured 2θ	Error 2θ	Measured 2θ	Corrected error 2θ	Corrected 2θ	'a' nm	$\frac{\cos^2\theta}{\sin\theta} + \frac{\cos^2\theta}{\theta}$	Additional peaks corrected 2θ
(220)	76.4495	76.3646	-0.0849	76.5650	-0.0850	76.6500	0.351609	1.9126	
(311)	93.0286	92.9363	-0.0924	93.1975	-0.0944	93.2919	0.351625	1.2270	
$(222)_{\alpha_1}$	98.4332	98.3300	-0.1032	98.5713	-0.1013	98.6726	0.351757	1.0529	93.683_{α_1}
$(222)_{\alpha_2}$	98.7631	98.6625	-0.1006	98.8725	-0.1004	98.9729	0.351838	1.0437	
$(331)_{\alpha_1}$	144.6407	144.5975	-0.4320	145.1650	-0.0545	145.2195	0.351828	0.1641	
$(331)_{\alpha_2}$	145.5433	145.4825	-0.0608	145.9238	-0.0608	145.9846	0.351972	0.1566	

Table 4.2.10 Calculation of 'a' Values for the Matrix Phase from Diffraction Pattern of Ni-14 at. % Si, aged at 700°C for 4 hrs.

Reflecting plane	Pure nickel			Ni-14 at. % Si alloy, aged at 700°C for 4 hrs.					
	Theoretical 2θ	Measured 2θ	Error 2θ	Measured 2θ	Corrected error 2θ	Corrected 2θ	'a' nm	$\frac{\cos^2\theta}{\sin\theta} + \frac{\cos^2\theta}{\theta}$	Additional peaks corrected 2θ
(200)	51.8916	51.8200	-0.0716	51.9175	-0.0717	51.9892	0.351774	3.6241	
$(220)_{\alpha_1}$	76.3752	76.2788	-0.0965	76.4200	-0.0956	76.5156	0.351842	1.9192	
$(220)_{\alpha_2}$	76.5989	76.5038	-0.0951	76.6350	-0.0952	76.7302	0.351880	1.9086	
$(311)_{\alpha_2}$	93.2286	93.1213	-0.1074	93.3013	-0.1074	93.4086	0.351868	1.2231	
$(222)_{\alpha_1}$	98.4332	98.3263	-0.1069	98.5063	-0.1083	98.6145	0.351910	1.0547	
$(222)_{\alpha_2}$	98.7631	98.6538	-0.1094	98.8225	-0.1093	98.9318	0.351946	1.0450	
$(331)_{\alpha_1}$	144.6407	144.5400	-0.1007	145.0688	-0.0893	145.1580	0.351887	0.1647	146.8308_{α_1}
$(331)_{\alpha_2}$	145.5433	145.4625	-0.0808	145.9063	-0.0808	145.9871	0.351970	0.1567	

Table 4.2.11 Calculation of 'a' Values for the Matrix Phase from Diffraction Pattern of Ni-14 at. % Si, Aged at 700°C for 10 hrs.

Reflecting plane	Pure nickel			Ni-14 at. % Si alloy, aged at 700°C for 10 hrs.					
	Theoretical 2θ	Measured 2θ	Error 2θ	Measured 2θ	Corrected error 2θ	Corrected 2θ	'a' nm	$\frac{\cos^2\theta}{\sin\theta} + \frac{\cos^2\theta}{\theta}$	Additional peaks corrected 2θ
(200)	51.8916	51.7900	-0.0557	51.9225	-0.0559	51.9784	0.351843	3.6251	Extra peaks could not be measured accurately
$(220)_{\alpha_1}$	76.3752	76.2850	-0.0902	76.4125	-0.0916	76.5041	0.351887	1.9198	
$(220)_{\alpha_2}$	76.5989	76.5063	-0.0926	76.6281	-0.0925	76.7206	0.351920	1.9091	
$(222)_{\alpha_1}$	98.4332	98.3600	-0.0732	98.5300	-0.0712	98.6012	0.351945	1.0551	
$(331)_{\alpha_1}$	144.6407	144.5925	-0.0482	145.0112	-0.0403	145.0515	0.351990	0.1658	
$(331)_{\alpha_2}$	145.5433	145.5125	-0.0308	145.9000	-0.0308	145.9308	0.352023	0.1572	

Table 4.2.12 Calculation of 'a' Values for the Matrix Phase from Diffraction Pattern of Ni-14 at. % Si, Aged at 700°C for 40 hrs.

Reflecting plane	Pure nickel			Ni-14 at. % Si alloy, aged at 700°C for 40 hrs.					
	Theoretical 2θ	Measured 2θ	Error 2θ	Measured 2θ	Corrected error 2θ	Corrected 2θ	'a' nm	$\frac{\cos^2\theta}{\sin\theta} + \frac{\cos^2\theta}{\theta}$	Additional peaks corrected 2θ
$(220)_{\alpha_1}$	76.3752	76.2750	-0.1002	76.4800	-0.0914	76.5714	0.351625	1.9165	
(311)	93.0286	92.9161	-0.1125	93.1743	-0.1067	93.2810	0.351656	1.2274	
$(222)_{\alpha_1}$	98.4332	98.3300	-0.1032	98.5518	-0.0998	98.6516	0.351812	1.0535	
$(222)_{\alpha_2}$	98.7631	98.6650	-0.0981	98.6687	-0.0950	98.9637	0.351862	1.0440	
$(331)_{\alpha_1}$	144.6407	144.5938	-0.0470	144.9849	-0.0481	145.0329	0.352008	0.1659	
$(331)_{\alpha_2}$	145.5433	145.4937	-0.0496	145.8710	-0.0496	145.9206	0.352033	0.1573	146.83_{α_1}

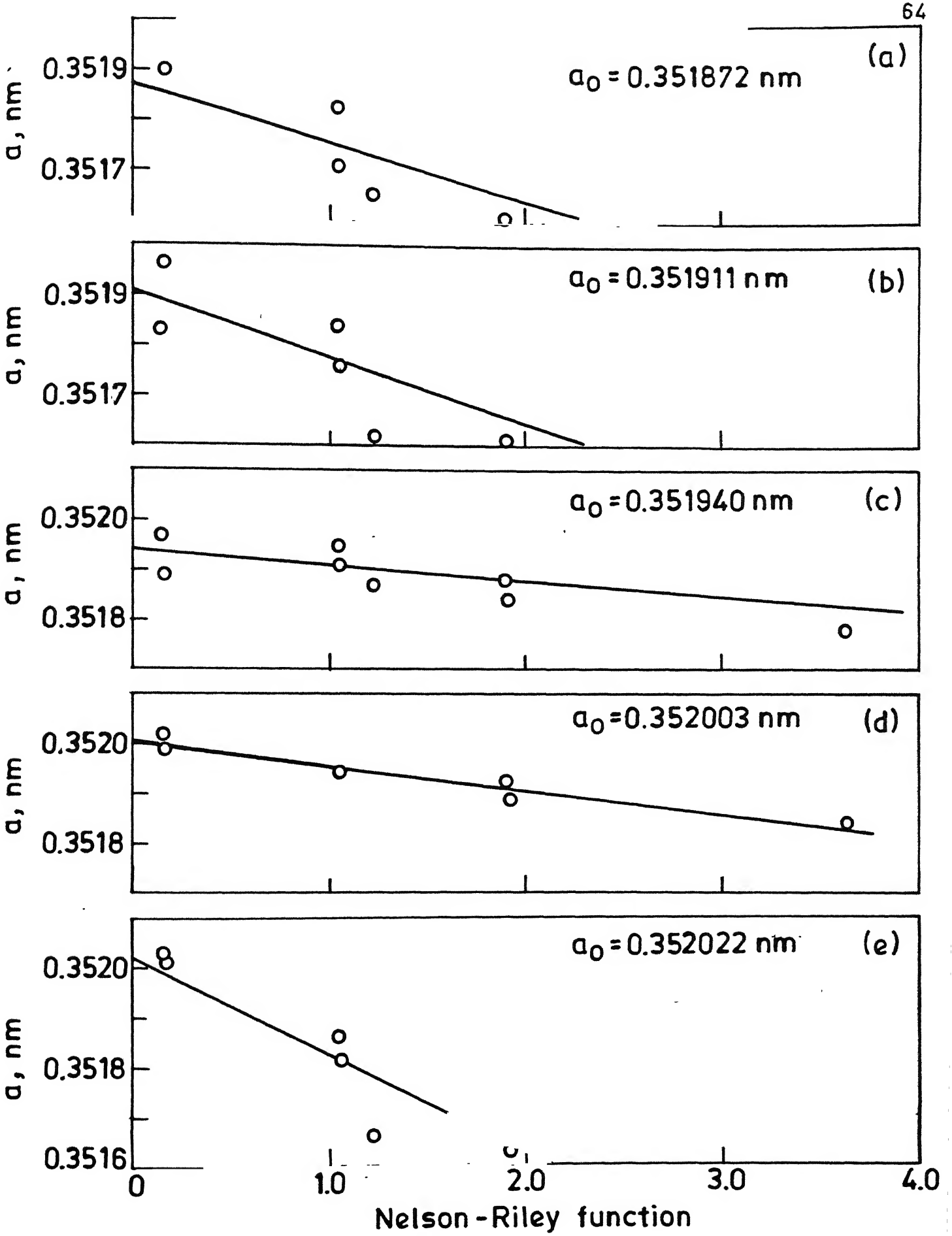

Fig. 4.2.4 Nelson-Riley plots for sample aged at 700°C for (a) 1 hr (b) 2 hrs (c) 4 hrs (d) 10 hrs (e) 40 hrs.

Table 4.2.13 Calculation of 'a' Values for the Matrix Phase from Diffraction Pattern of Ni-14 at. % Si, Aged at 650°C for 92 hrs.

Reflecting plane	Pure nickel			Ni-14 at. % Si alloy, aged at 650°C for 92 hrs.					
	Theoretical 2θ	Measured 2θ	Error 2θ	Measured 2θ	Corrected error 2θ	Corrected 2θ	'a' nm	$\frac{\cos^2\theta}{\sin\theta} + \frac{\cos^2\theta}{\theta}$	Additional peaks corrected 2θ
$(220)_{\alpha_1}$	76.3752	76.2294	-0.1458	76.3676	-0.1565	76.5242	0.351809	1.9185	
$(220)_{\alpha_2}$	76.5989	76.4375	-0.1614	76.5621	-0.1611	76.7232	0.351906	1.9091	
$(311)_{\alpha_1}$	92.9292	92.8063	-0.1229	92.9919	-0.1265	93.1184	0.351838	1.2330	
$(222)_{\alpha_1}$	98.4332	98.3087	-0.1245	98.5101	-0.1196	98.6297	0.351870	1.0542	99.2026_{α_1}
$(222)_{\alpha_2}$	98.7631	98.6468	-0.1163	98.8231	-0.1162	98.9393	0.351926	1.0447	99.5069_{α_2}
$(331)_{\alpha_1}$	144.6407	144.5264	-0.1143	145.1339	-0.1018	145.2357	0.351812	0.1639	146.915_{α_1}
$(331)_{\alpha_2}$	145.5433	145.4479	-0.0954	145.9543	-0.0954	146.0497	0.351911	0.1553	

Table 4.2.14 Calculation of 'a' Values for the Matrix Phase from Diffraction Pattern of Ni-14 at. % Si, Aged at 650°C for 165 hrs.

Reflecting plane	Pure nickel			Ni-14 at. % Si alloy, aged at 650°C for 165 hrs.					
	Theoretical 2θ	Measured 2θ	Error 2θ	Measured 2θ	Corrected error 2θ	Corrected 2θ	'a' nm	$\frac{\cos^2\theta}{\sin\theta} + \frac{\cos^2\theta}{\theta}$	Additional peaks corrected 2θ
$(220)_{\alpha_1}$	76.3752	76.2547	-0.1205	76.3656	-0.1198	76.4853	0.351960	1.9207	
$(311)_{\alpha_1}$	92.9292	92.8147	-0.1145	92.9962	-0.1163	93.1125	0.351856	1.2332	93.6224_{α_1}
$(222)_{\alpha_1}$	98.4332	98.3182	-0.1150	98.5082	-0.1078	98.6160	0.351906	1.0546	99.2379_{α_1}
$(222)_{\alpha_2}$	98.7631	98.6610	-0.1021	98.8205	-0.1021	98.9226	0.351970	1.0452	
$(331)_{\alpha_1}$	144.6407	144.5535	-0.0872	145.0800	-0.0922	145.1722	0.351874	0.1646	146.9297_{α_1}
$(331)_{\alpha_2}$	145.5433	145.4476	-0.0957	145.9700	-0.0957	146.0657	0.351896	0.1558	147.8947_{α_2}

Table 4.2.15 Calculation of 'a' values for the matrix phase from diffraction pattern of Ni-14 at.% Si, aged at 650°C for 198 hrs.

Reflecting plane	Pure nickel			Ni-14 at. % Si alloy, aged at 650°C for 198 hrs.					
	Theoretical 2θ	Measured 2θ	Error 2θ	Measured 2θ	Corrected error 2θ	Corrected 2θ	'a' nm	$\frac{\cos^2\theta}{\sin\theta} + \frac{\cos^2\theta}{\theta}$	Additional peaks corrected 2θ
(220)	76.4495	76.3590	-0.0905	76.4350	-0.0904	76.5254	0.352094	1.9187	
$(311)_{\alpha_1}$	92.9292	92.8452	-0.0840	92.9700	-0.0879	93.0579	0.352015	1.2351	
$(222)_{\alpha_1}$	98.4332	98.3193	-0.1139	98.4611	-0.1120	98.5731	0.352019	1.0559	$(99.208)_{\alpha_1}$
$(222)_{\alpha_2}$	98.7631	98.6537	-0.1094	98.7877	-0.1094	98.8971	0.352037	1.0460	
$(331)_{\alpha_1}$	144.6407	144.5714	-0.0693	145.0388	-0.0625	145.1012	0.351942	0.1653	$(146.9299)_{\alpha_1}$
$(331)_{\alpha_2}$	145.5433	145.4874	-0.0559	145.9375	-0.0559	145.9934	0.351964	0.1566	

Table 4.2.16 Calculation of 'a' Values for the Matrix Phase from Diffraction Pattern of Ni-14 at.% Si, Aged at 600°C for 22 hrs.

Reflecting plane	Pure nickel			Ni-14 at.% Si alloy, aged at 600°C for 22 hrs.					
	Theoretical 2θ	Measured 2θ	Error 2θ	Measured 2θ	Corrected error 2θ	Corrected 2θ	'a' nm	$\frac{\cos^2\theta}{\sin\theta} + \frac{\cos^2\theta}{\theta}$	Additional
(220)	76.4495	76.3940	-0.0555	76.4875	-0.0556	76.5431	0.352025	1.9178	No extra
(311)	93.0286	92.9498	-0.0788	93.1225	-0.0781	93.2006	0.351889	1.2302	peak could
$(222)_{\alpha_1}$	98.4332	98.3750	-0.0582	98.5477	-0.0565	98.6042	0.351937	1.0549	be detected
$(222)_{\alpha_2}$	98.7631	98.7081	-0.0550	98.8555	-0.0550	98.9105	0.352002	1.0456	
$(331)_{\alpha_1}$	144.6407	144.5501	-0.0906	145.2050	-0.0881	145.2931	0.351757	0.1634	
$(331)_{\alpha_2}$	145.5433	145.4556	-0.0877	145.9325	-0.0877	146.0202	0.351939	0.1563	

Table 4.2.17 Calculation of 'a' Values for the Matrix Phase from Diffraction Pattern of Ni-14 at% Si, Aged at 600°C for 85 hrs.

Reflecting plane	Pure nickel			Ni-14 at % Si alloy, aged at 600°C for 85 hrs.					
	Theoretical 2θ	Measured 2θ	Error 2θ	Measured 2θ	Corrected error 2θ	Corrected 2θ	'a' nm	$\frac{\cos^2\theta}{\sin\theta} + \frac{\cos^2\theta}{\theta}$	Extra peaks 2θ corrected
(200)	51.8916	51.8092	-0.0824	51.8700	-0.0825	51.9525	0.352006	3.6277	
$(220)_{\alpha_1}$	76.3752	76.2707	-0.1045	76.3925	-0.1049	76.4974	0.351913	1.9201	
$(220)_{\alpha_2}$	76.5989	76.4937	-0.1052	76.6013	-0.1051	76.7064	0.351972	1.9098	
$(311)_{\alpha_1}$	93.9292	92.8317	-0.0975	93.0050	-0.0996	93.1046	0.351879	1.2335	99.2197α_2 99.5888α_1
$(331)_{\alpha_1}$	144.6407	144.5400	-0.1007	145.1382	-0.0919	145.2301	0.351818	0.1640	123.1602
$(331)_{\alpha_2}$	145.5433	145.4561	-0.0872	146.0050	-0.0872	146.0922	0.351871	0.1557	

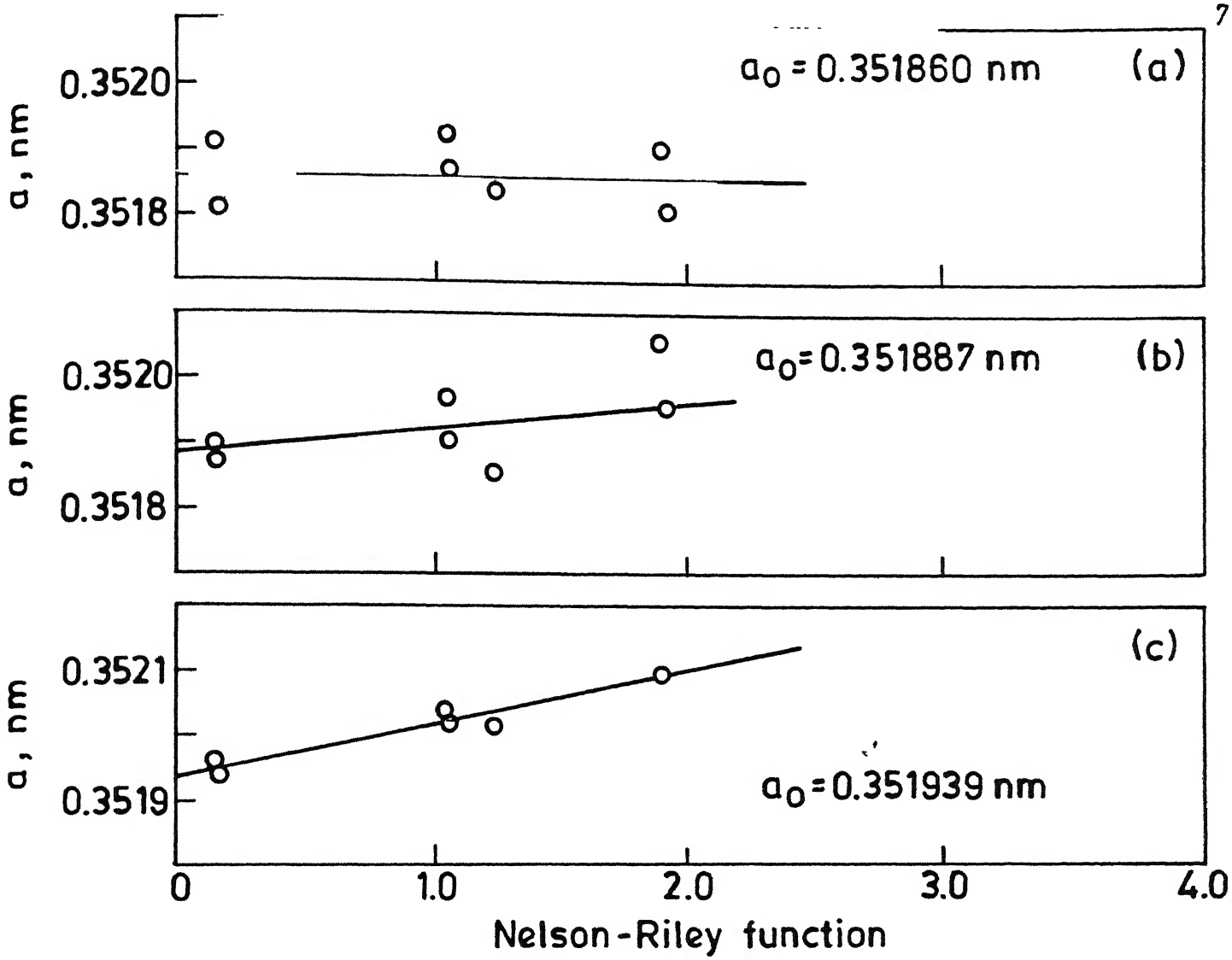

Fig. 4.2.5 Nelson-Riley plots for sample aged at 650°C for for (a) 92 hrs (b) 165 hrs (c) 198 hrs.

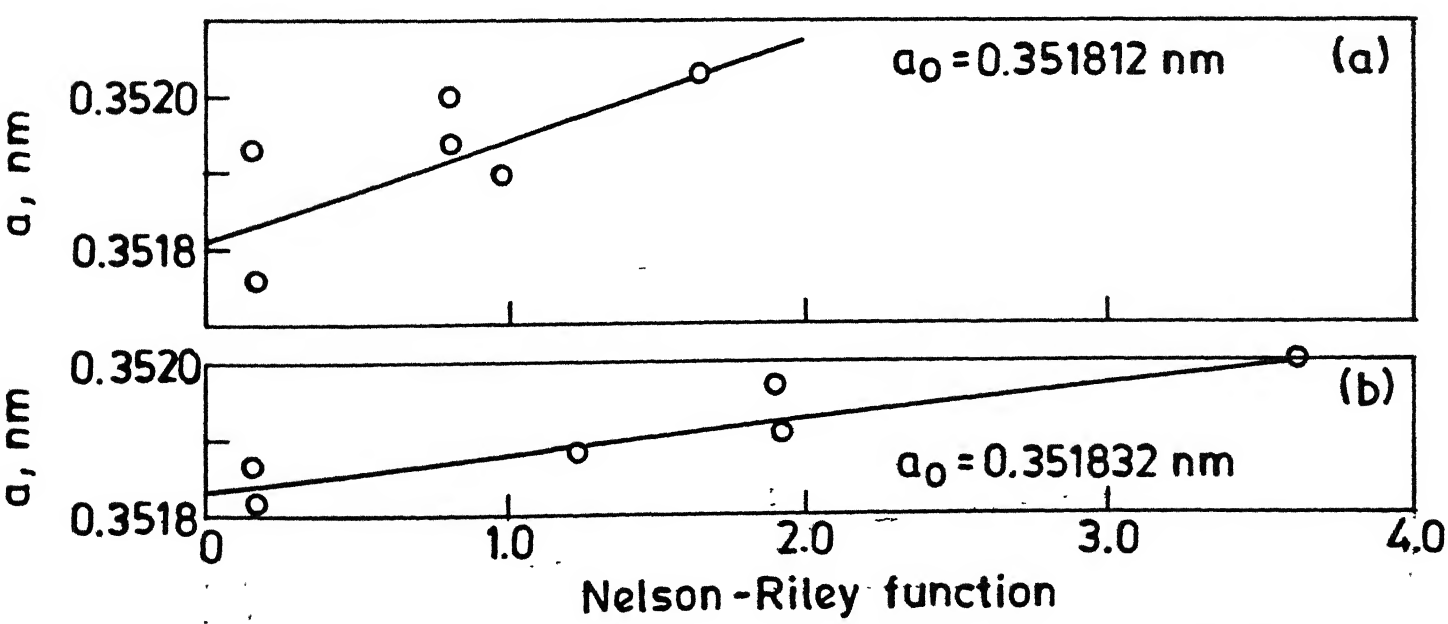

Fig. 4.2.6 Nelson-Riley plots for sample aged at 600°C for (a) 22 hrs (b) 85 hrs.

Chapter V

Discussions

5.1 Solvus of the Ni-rich Solid Solution

The lattice parameter of Ni-14 at. % Si alloy measured in this investigation has been plotted in Figure 5.1.1 along with all available data. The result of this investigation is in good agreement with available data.

The lattice parameters of aged alloys are plotted against aging time in Figure 4.2.2. At two temperatures, 700 and 750°C, it clearly shows that the lattice parameter of matrix phase approaches a constant value after some time. These constant values must correspond to the solid solutions which is in equilibrium with the precipitate at these aging temperatures. Figure 5.1.1 is a plot of lattice parameter versus composition. From this plot the composition of the matrix in equilibrium with the precipitate at the above aging temperatures were obtained. Recently the solubility of Ni_3Si in the Ni-rich solid solution have been measured by Oya and Suzuki.[8] Their values are 14.0at. % at 1015 °C and 12.0 at. % at 940°C. Values obtained from this investigation have been plotted in Figure 5.1.2 along with the results of Oya and Susuki.[8] The figure shows a smooth solvus line. The eutectoid temperature of 1035°C shown in this figure is due to Oya and Suzuki.[8]

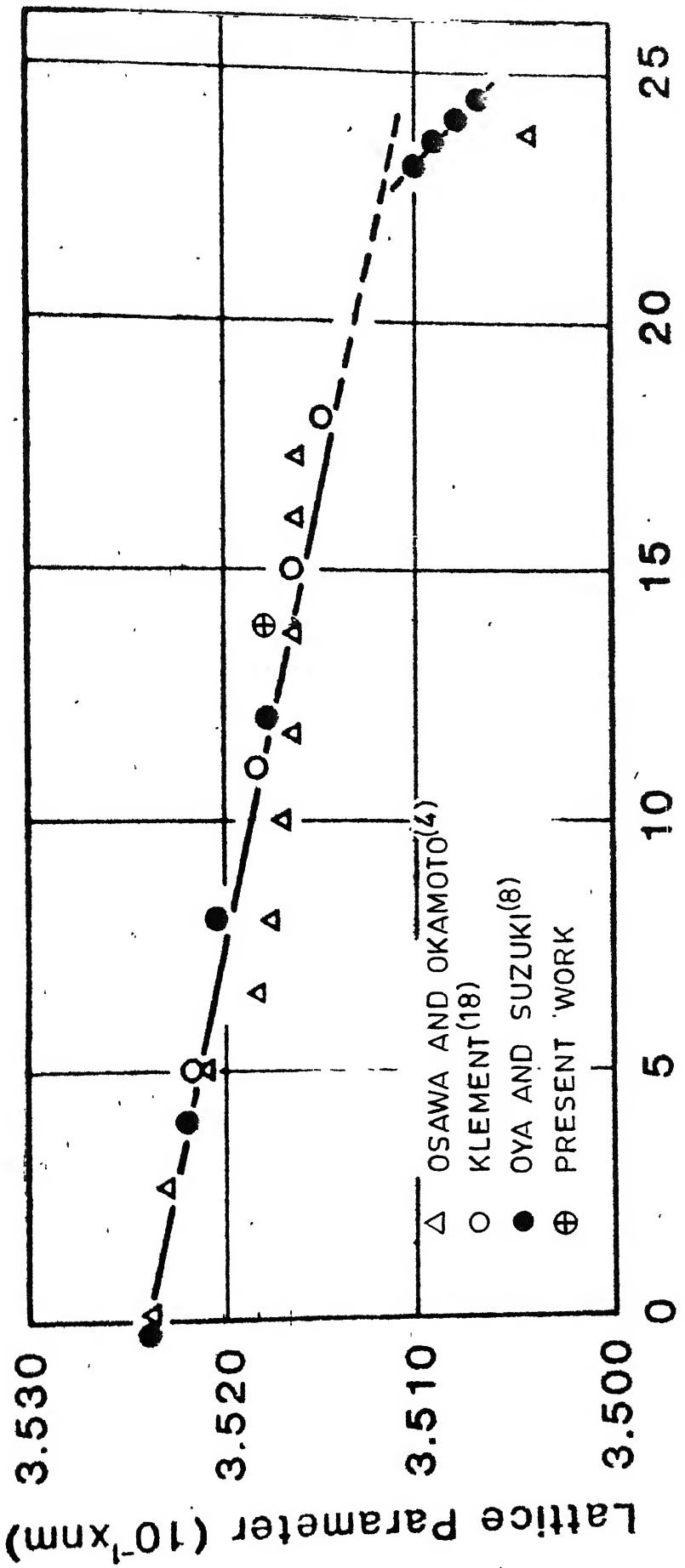

Fig. 5.1.1 Composition dependence of lattice parameter of the Ni-Si primary solid solution and the Ni_3Si β_1 phase.

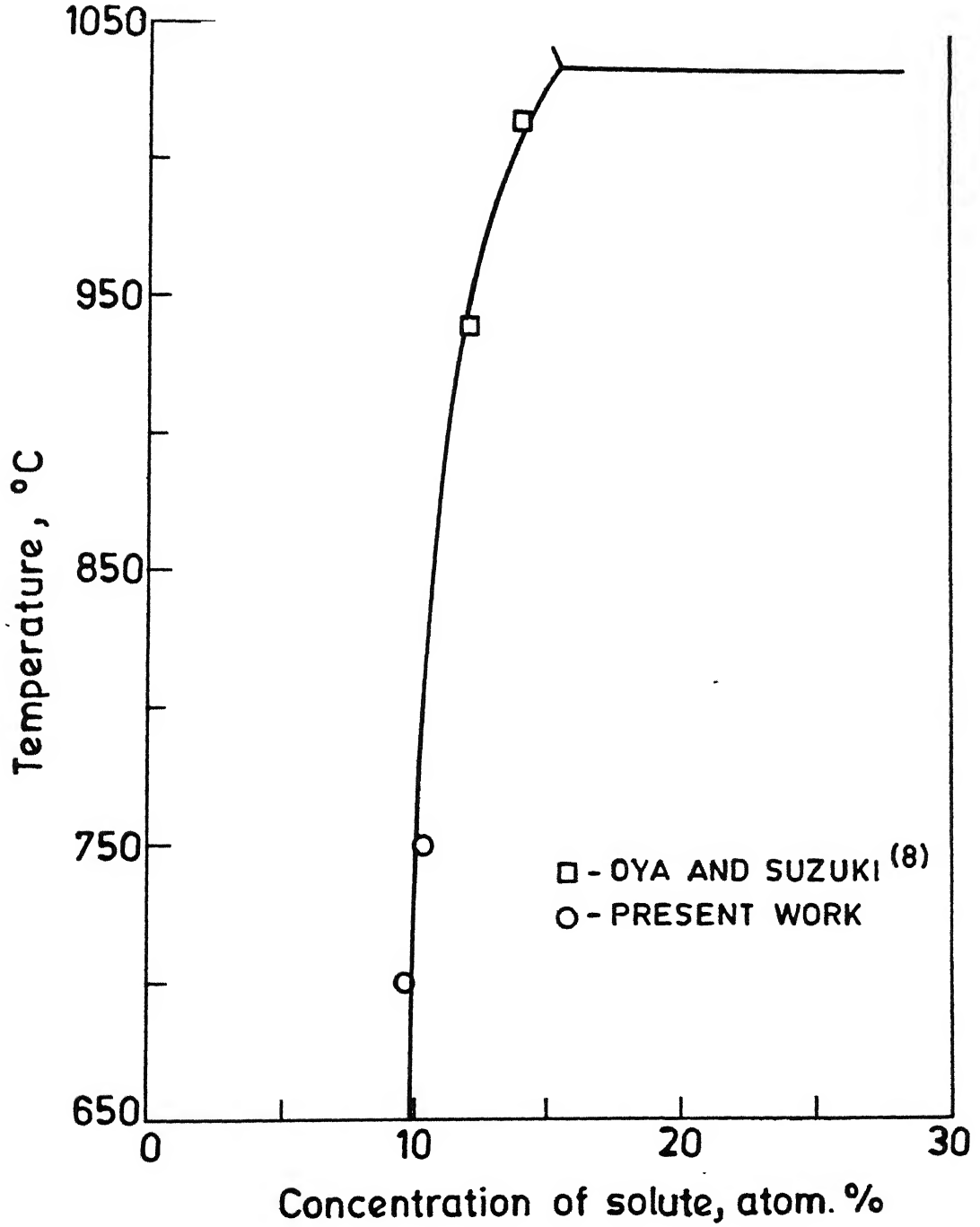

Fig. 5.1.2 Solvus curve on nickel rich side in Ni-Si system.

5.2 Equilibrium between Ni_3Si and Ni-Si Solid Solution

The latest phase diagram due to Oya and Suzuki[8] shows that the composition of Ni_3Si which is in equilibrium with Ni-rich solid solution at 827°C is 22.7 at. % Si and the trend at lower temperatures is for this composition to remain constant.

The equilibrium between $Ni_{0.773}Si_{0.227}$ and the solid solution may be represented by the following equation

$$0.773\ Ni\ (\text{in solid solution}) + 0.227\ Si\ (\text{in solid solution}) = Ni_{0.773}Si_{0.227}$$

Hence the equilibrium constant

$$K = \frac{a_{Ni_{0.773}Si_{0.227}}}{a_{Ni}^{0.773} \cdot a_{Si}^{0.227}}$$

Taking the activity of $Ni_{0.773}Si_{0.227}$ to be 1 and taking the activity coefficients to be ,

$$K = \frac{1}{\gamma_{Ni}^{0.773} \cdot X_{Ni}^{0.773} \cdot \gamma_{Si}^{0.227} \cdot X_{Si}^{0.227}}$$

Since the composition of the solid solution in equilibrium with $Ni_{0.773}Si_{0.227}$ varies within 6 at. % Si, the activity coefficients are assumed to be constant.

Hence the standard free energy change, G° is given by the following equation

$$\Delta G^\circ = - RT \ln K = + RT \ln(\gamma_{Ni}^{0.773} \cdot \gamma_{Si}^{0.227}) + RT \ln(X_{Ni}^{0.773} \cdot X_{Si}^{0.227})$$

or

$$\Delta H^{\circ} - T\Delta S^{\circ} - RT \ln(\gamma_{Ni}^{0.773} \cdot \gamma_{Si}^{0.227})$$

$$= RT \ln(X_{Ni}^{0.773} \cdot X_{Si}^{0.227})$$

$$0.773 \log X_{Ni} + 0.227 \log X_{Si}$$

$$= \frac{\Delta H^{\circ}}{2.303\ RT} - \left(\frac{\Delta S^{\circ} + R \ln \gamma_{Ni}^{0.773} \cdot \gamma_{Si}^{0.227}}{2.303\ R}\right)$$

$$\log X_{Si} + \left(\frac{0.773}{0.227}\right) \log X_{Si}$$

$$= \frac{\Delta H^{\circ}}{(0.227)(2.303)RT} - \left(\frac{\Delta S^{\circ} + R \ln \gamma_{Ni}^{0.773} \cdot \gamma_{Si}^{0.227}}{(0.227)(2.303\ R)}\right)$$

Plotting $(\log X_{Si} + \frac{0.773}{0.227} \log X_{Ni})$ against 1/T, one can determine the standard enthalpy of formation (ΔH°) of the compound $Ni_{0.773}Si_{0.227}$. The values of $(\log X_{Si} + (\frac{0.773}{0.227}) \log X_{Ni})$ and 1/T are listed in Table 5.2.1 and the plot is shown in Figure 5.2.1. The slope gives the value of -351 cal/mole as the standard enthalpy of formation of $Ni_{0.773}Si_{0.227}$. This is in very good agreement with standard enthalpy of formation of 200 cal/mole determined by Jena and RamBrahma[16] of $Ni_{0.775}Ge_{0.225}$.

5.3 Hardening Effect of Silicon in Ni-Si Solid Solution

The plot of change of flow stress against change of Lattice Parameters for a number of Ni-base alloys as studied by Grant et al[65] is shown in Fig. 5.3.1. Jena and RamBrahma[16] demonstrated that change of microhardness with change in Δa_o is

Table 5.2.1 Experimental Values of X_{Si} and the Corresponding Solvus Temperature

Temperature	X_{Si}	$\log X_{Si} + (\frac{0.773}{0.227}) \log X_{Ni}$	$1/T\ (^{\circ}K^{-1})$
700°C	0.0971	-1.1638	10.277×10^{-4}
750°C	0.1038	-1.1459	9.775×10^{-4}
940°C	0.1200	-1.1099	8.244×10^{-4}
1015°C	0.1400	-1.0769	7.764×10^{-4}

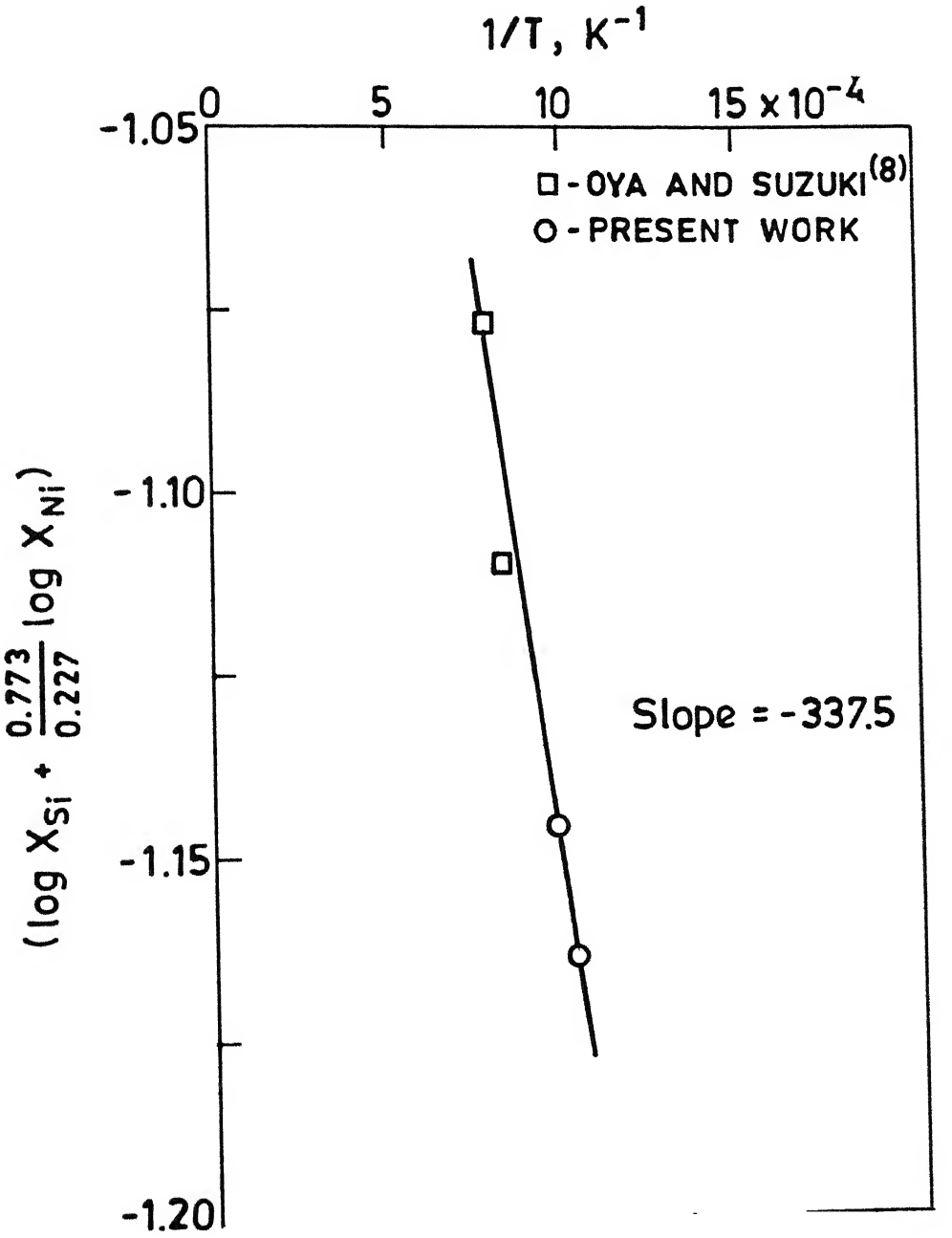

Fig. 5.2.1 Calculation of the standard enthalpy of formation of $Ni_{0.773}Si_{0.227}$.

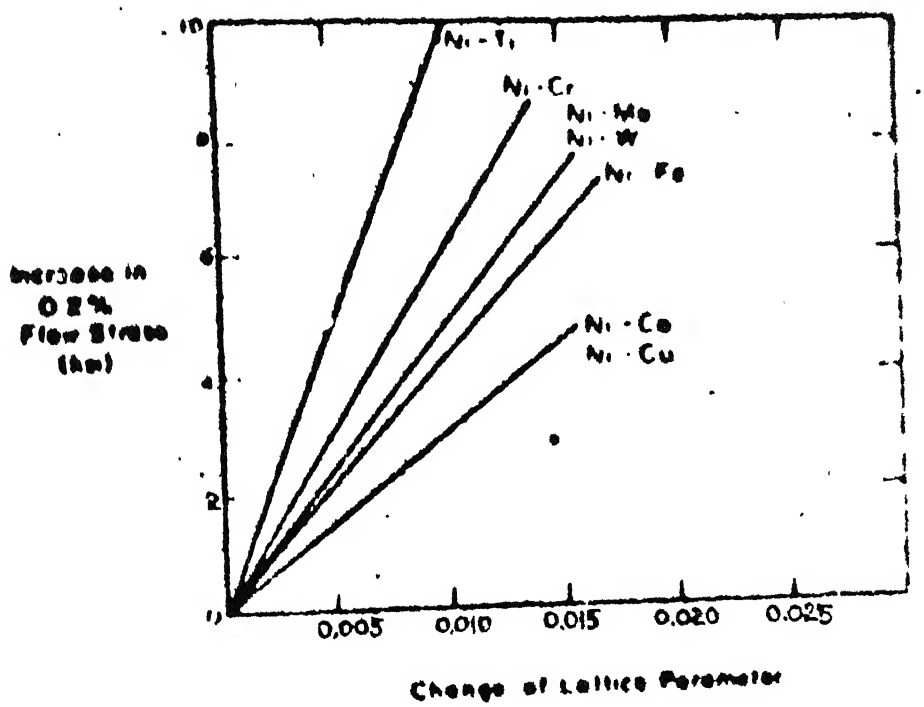

Fig.5.3.1 : Plot of change of flow stress vs change in lattice parameter for various Ni-base alloys[65]

also linear with Ni-Ge alloys (Figure 5.3.2). It has been suggested that elements having same electronic structure should have same hardening effect. However, change of hardness against Δa plots for Ni-Ge,[16] Ni-Sn[66] and Ni-Si alloys cannot be represented by a single line as shown in Figure 5.3.2. A plot of change of hardness versus composition shown in Figure 5.3.3 clearly demonstrates that the hardening effect due to tetravalent elements Si, Ge[16] and Sn[66] with considerable covalent bonding depends simply on the atomic percent of the alloying elements.

When these solutes are present in the solid solution, the atomic configuration around the solutes are considerably disturbed which leads to increase resistance to the motion of dislocations and consequently to the increase in hardness. It is, therefore, expected that these elements would have similar effects on hardening.

5.4 Kinetics of Precipitation

Figure 5.1.1 shows that lattice parameter is a linear function of solute concentration C. Thus

$$a = A + BC \qquad (5.4.1)$$

where A and B are constants.

The volume fraction of precipitate Y may be expressed as

$$Y = \left(\frac{C_o - C}{C_o - C_e}\right) \qquad (5.4.2)$$

where C_o = concentration of solute in the alloy

C = concentration of solute at any time 't'

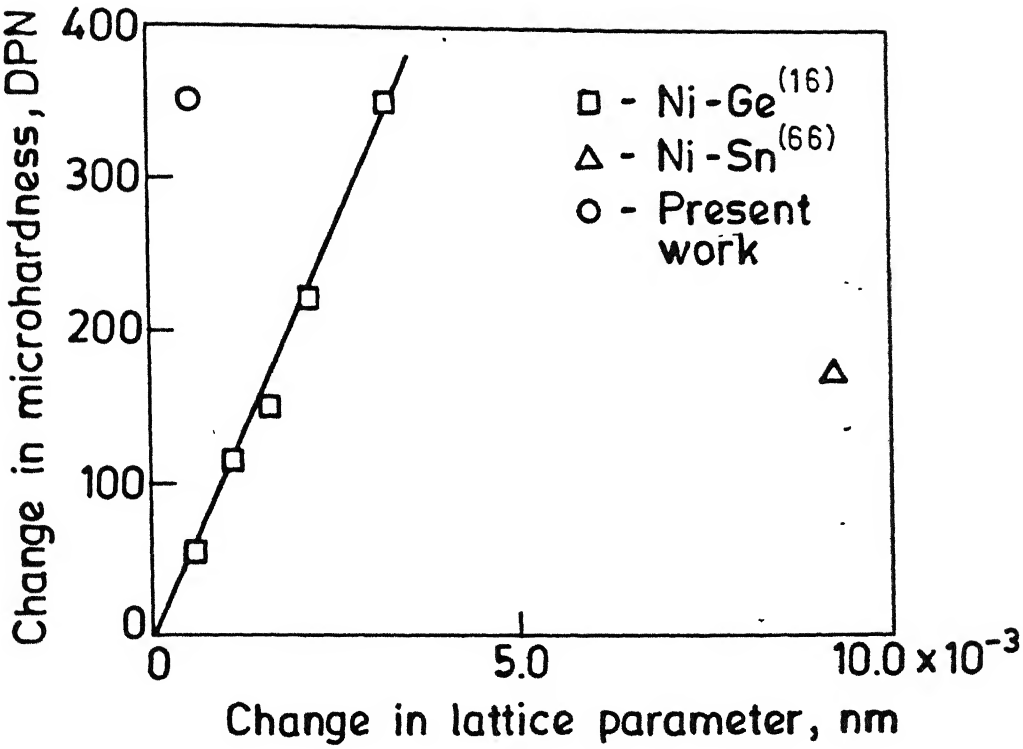

Fig. 5.3.2 Increase in microhardness values with change in lattice parameter.

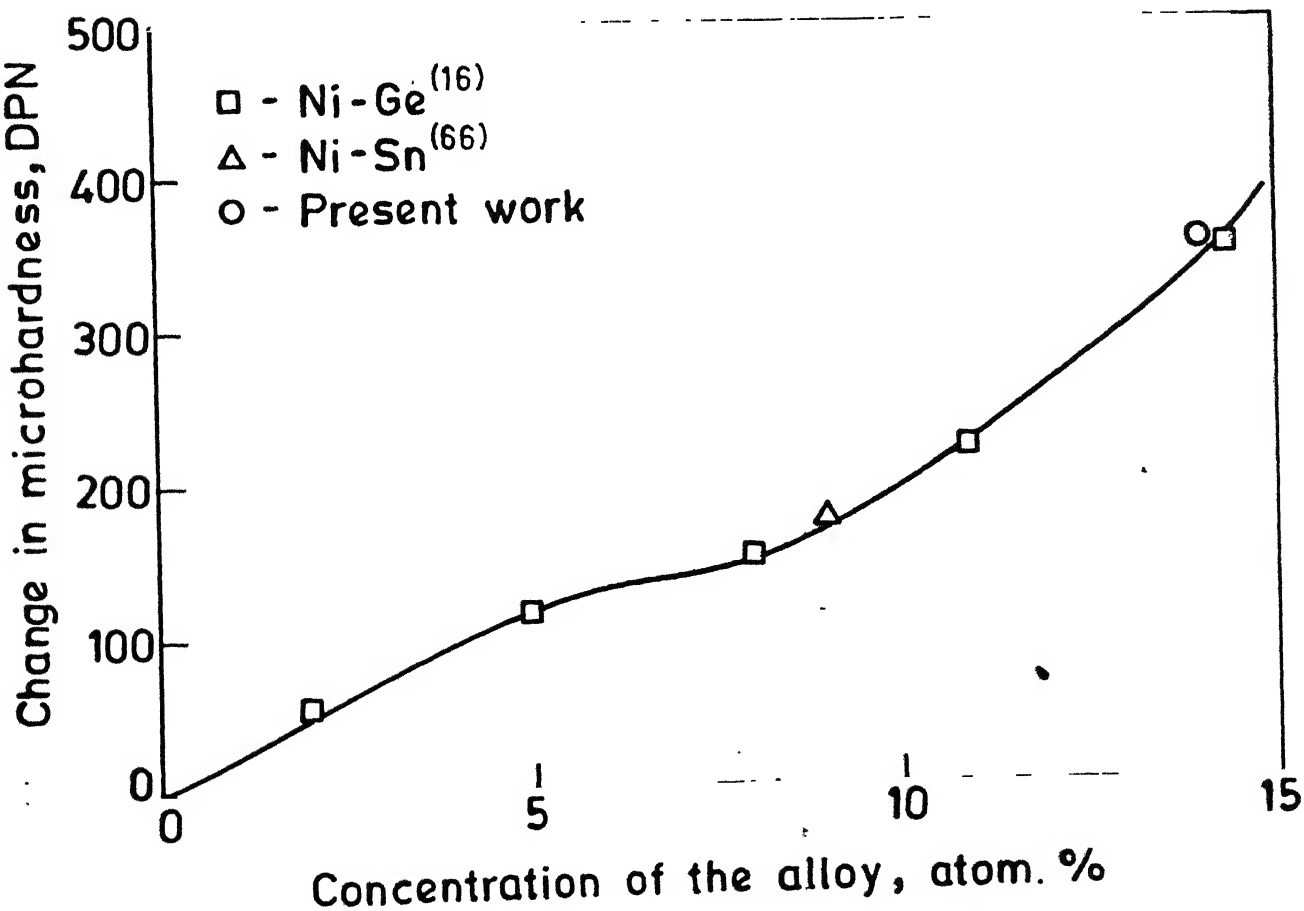

Fig. 5.3.3 Increase in microhardness values with composition.

C_e = concentration of solute at equilibrium.

Combining equations (5.4.1) and (5.4.2), one can show that

$$Y = \left(\frac{a_o - a}{a_o - a_e}\right) \qquad (5.4.3)$$

The transformation behaviour can in general be expressed by the Johnson-Mehl type of equation[66]

$$Y = 1 - e^{-Kt^n} \qquad (5.4.4)$$

where K and n are constants, and t is time of transformation. The equation (5.4.4) can be written as the equation below:

$$\log \log\left(\frac{1}{1 - Y}\right) = \log\left(\frac{K}{2.3026}\right) + n \log t \qquad (5.4.5)$$

The Figure 4.2.2 showing variation of 'a' with aging time shows that aging at 700°C and 750°C have resulted in attainment of equilibrium and the lattice parameters of the matrix 0.352022 and 0.351975 nm respectively can be taken as the lattice parameters at equilibrium. Thus it is possible to calculate Y from equation (5.4.3). The values of Y so calculated have been listed in Table 5.4.1 and are plotted in Figure 5.4.1 after equation (5.4.5). The slope obtained from these plots is 0.83 in both the cases. The value of K obtained are 3.63×10^{-4} at 700°C and 1.26×10^{-4} at 750°C. These plots and the low scatter show that the data are internally consistant.

The data corresponding to 850, 650 and 600°C cannot be treated in this manner as values of 'a_e' are not known. However, these represent the initial stages of transformation

Table 5.4.1 Volume Fraction of Precipitates at 700 and 750°C for various Times

Temp (°C)	Volume Percent of 'Y'	log log $(\frac{1}{1-Y})$	log t (sec.)
700°C	29.2	-0.82320	3.5563
	47.6	-0.55127	3.8573
	61.3	-0.38455	4.1584
	91.0	+0.02019	4.5563
750°C	48.5	-0.5025	3.5563
	60.6	-0.3930	3.8573
	82.4	-0.1220	4.5563

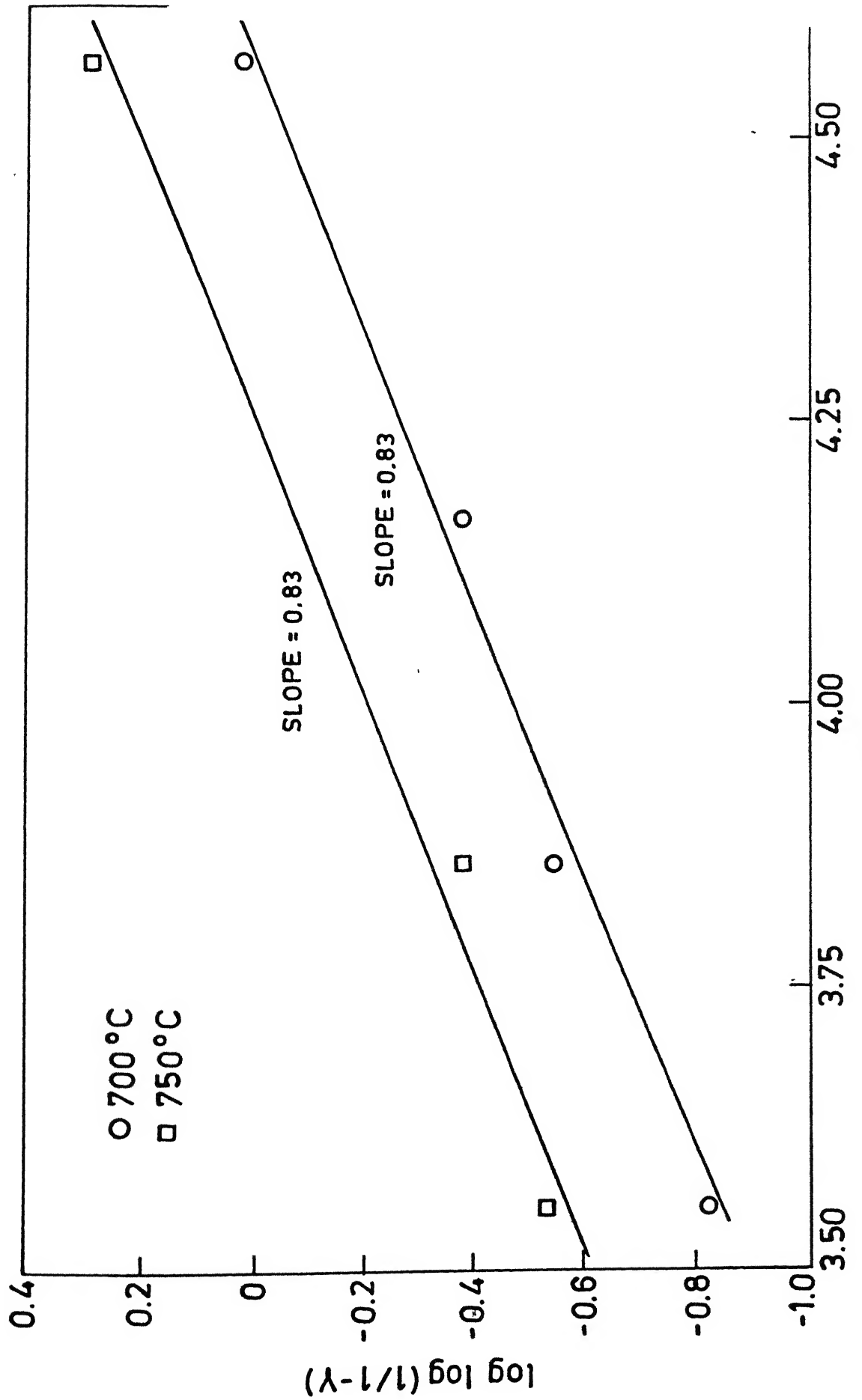

Fig. 5.4.1 Johnson-Mehl plots after equation (5.4.5).

where Y is very small. Under these conditions of small Y, ln(1 - Y) could be expanded and equation (5.4.4) may be reduced to the following form

$$Y = Kt^n \qquad (5.4.6)$$

or $$\log Y = \log K + n \log t \qquad (5.4.7)$$

Combination equation (5.4.7) with equation (5.4.3), one obtains as the equation below

$$\log(a - a_o) = \log K(a_e - a_o) + n \log t \qquad (5.4.8)$$

The data at 850, 650 and 600°C are listed as $(a - a_o)$ and 't' in Table 5.4.2 and are plotted after equation (5.4.8) in Figure 5.4.2, which shows that the data are again internally consistant and have low scattered. The values of 'n' and are 0.83 and 2.4×10^{-4} respectively.

Diffusion controlled precipitates on spherical particles should lead to value of 1.5 for 'n'. However, the value of 0.83 obtained in all cases suggests that other diffusion mechanisms may also be involved. However, the fact that same value of 'n' obtained for entire time range of precipitation and the same mechanism operates over the entire range, metastable phases do not form during precipitation.

The rate of precipitation changes appreciable from temperature to temperature as shown in Figure 4.2.2. The time required at any given temperature for obtaining 5% of the product has been plotted in Figure 5.4.3. Data for this figure are obtained in the following manner.

Table 5.4.2 Calculation of log $(a-a_o)$ and log t after Johnson-Mehl Equation (5.4.8)

Temp.(°C)	log $(a-a_o)$	log t (sec.)
600°C	-5.700	4.899
	-4.658	5.486
650°C	-4.301	5.520
	-4.114	5.774
	-3.889	5.853
850°C	-4.260	4.857
	-4.000	5.136

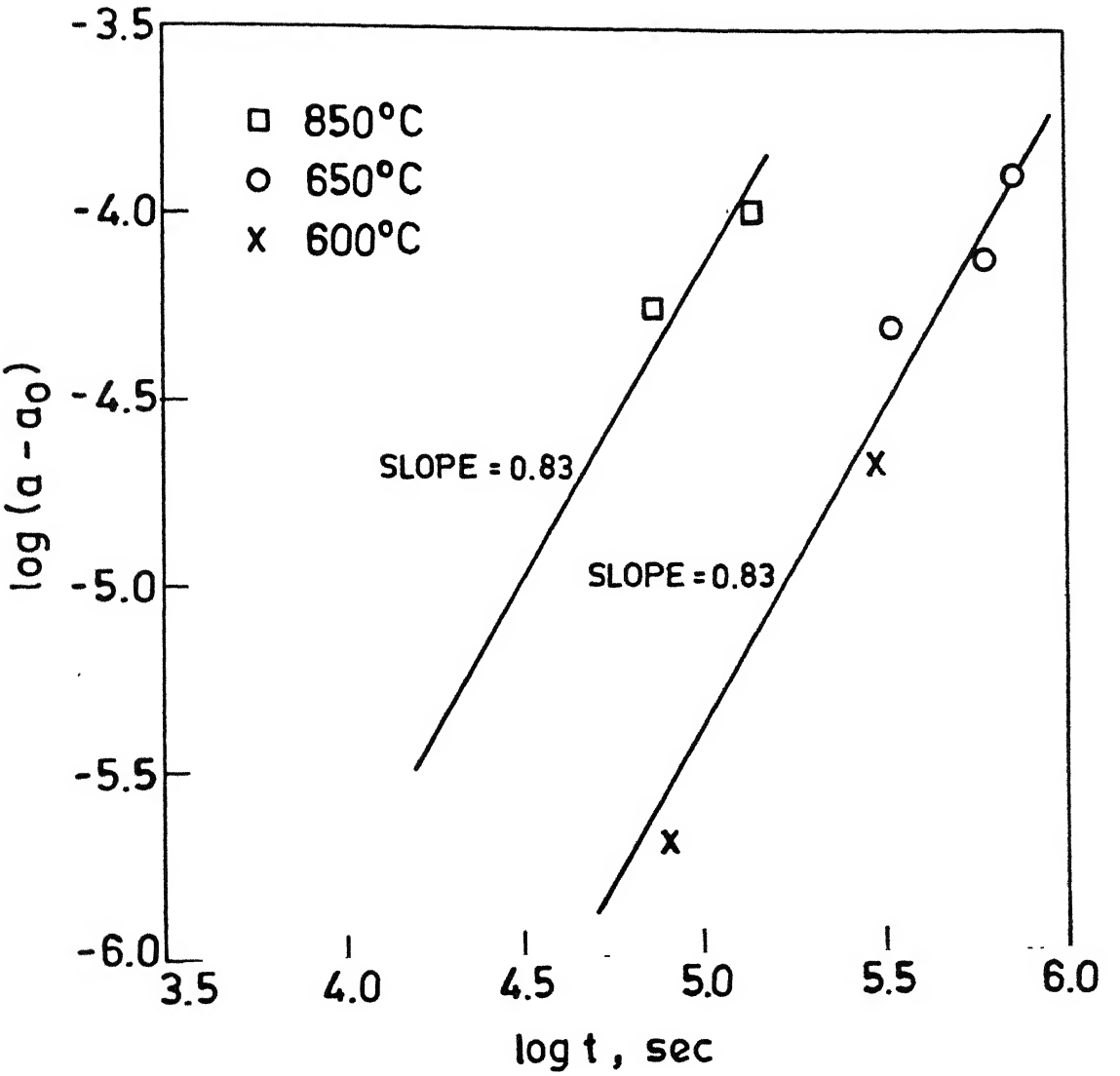

Fig. 5.4.2 Johnson-Mehl plots after equation (5.4.8)

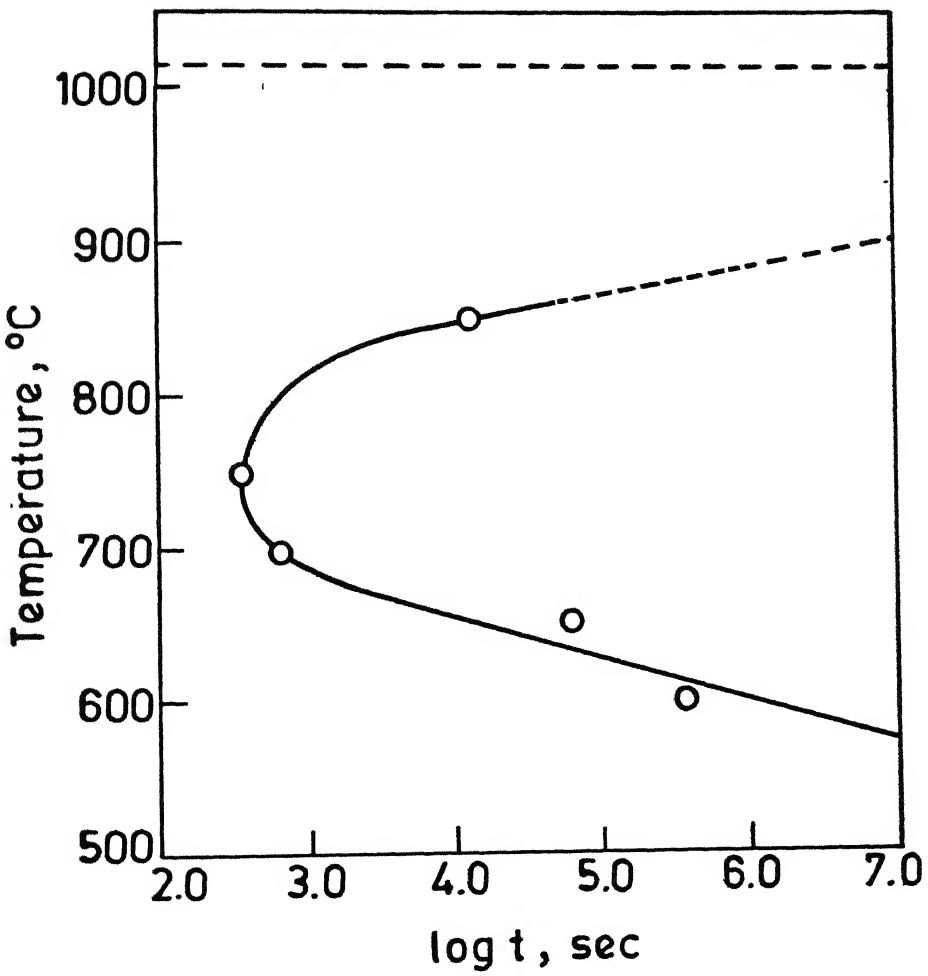

Fig. 5.4.3 Calculated C-curve for 5 pct. transformation of precipitated phase Ni_3Si.

Time for obtaining 5% of transformation may be expressed as

$$t = \frac{0.05}{(dY/dt)} \qquad (5.4.9)$$

This equation may also be expressed in terms of 'a' in the following manner

$$t = \alpha \cdot \frac{0.05}{(da/dt)} \qquad (5.4.10)$$

where α is a constant.

The values of 't' for 700°C and 750°C are obtained using equation (5.4.9) and are plotted in Figure 5.4.3. Also initial da/dt are obtained for 700° and 750°C and these are combined with 't' for Y = 0.05 and values of 'α' are calculated from equation (5.4.10). Using these values of 'α' and initial da/dt for 850, 650 and 600°C aging, the values of 't' were calculated and plotted in Figure 5.4.3. The figure also shows the solvus temperature obtained from the latest phase diagram given by Oya and Suzuki.[8]

This figure clearly shows a perfect expected c-curve type of behaviour and explains the apparent unusual variation of the rate of precipitation with temperature.

5.5 The Precipitating Phase

The additional peaks obtained after precipitation correspond to the reflections from $L1_2$ Ni_3Si. The corresponding lattice parameters have been shown in Table 5.5.1. Some of them have been plotted against the corresponding

Nelson-Riley functions in Figures.5.5.1, 5.5.2 and 5.5.3. The best 'a' values are listed in Table 5.5.2.

The value of lattice parameter 0.35022 nm obtained from this study is in excellent agreement with the lattice parameters from the literature of Osawa and Okamoto[4] as 0.3503 nm (23.8 at. % Si), Badtiev[35] as 0.3504 nm and of Labili[24] as 0.3505 nm (24-26 at. % Si).

The precipitate distribution is clearly shown in Figure 4.1.1 taken after aging at 750°C for 70 and 241 hrs., at 700°C for 40 hrs., at 650°C for 7 hrs. and at 600°C for 22 hrs. Electron microscopy observations by Chakraborty and Hornbogen[7] has confirmed that Ni_3Si forms coherently. The mismatch between Ni_3Si and Ni-14 at. % Si is only 0.45%. It is therefore expected that these particles appear coherently. They also observed spherical particles at 600 and 750°C. In this investigation scanning electron micrographs of samples aged at 750°C for 70 hrs., 700°C for 40 hrs. and at 600°C for 22 hrs. seems to be spherical. The precipitates are very fine in early stages, therefore, could not be observed.

Table 5.5.1 Calculation of 'a' Values for the Precipitate Phase β_1-Ni_3Si from Extra Peaks Obtained with Samples Aged After Quenching from Homogenization Temperature

Reflecting plane	Aging temperature and time												
	850°C		750°C				700°C			650°C			600°C
	20 hrs.	38 hrs.	1 hr.	2 hrs.	10 hrs.	310 hrs.	2 hrs.	4 hrs.	40 hrs.	92 hrs.	165 hrs.	198 hrs.	85 hrs.
$(220)_{\alpha_1}$		0.3503				0.3501							
$(311)_{\alpha_1}$		0.3503				0.3503	0.3502				0.3504		
$(311)_{\alpha_2}$		0.3502											
$(222)_{\alpha_1}$	0.3503	0.3503	0.3503	0.3505	0.3504					0.3504	0.3503	0.3503	0.3503
$(222)_{\alpha_2}$				0.3504						0.3504			0.3502
$(400)_{\alpha_1}$													0.3503
$(331)_{\alpha_1}$			0.3503	0.3503		0.3503		0.3503	0.3503	0.3502	0.3502	0.3502	
$(331)_{\alpha_2}$											0.3502		

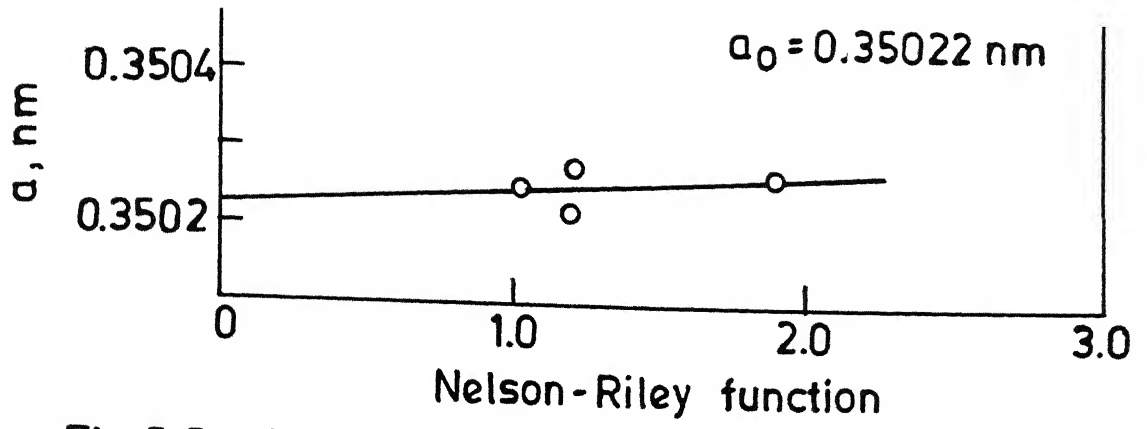

Fig. 5.5.1 Lattice parameter of pracipitated phase of sample aged at 850°C for 38 hrs.

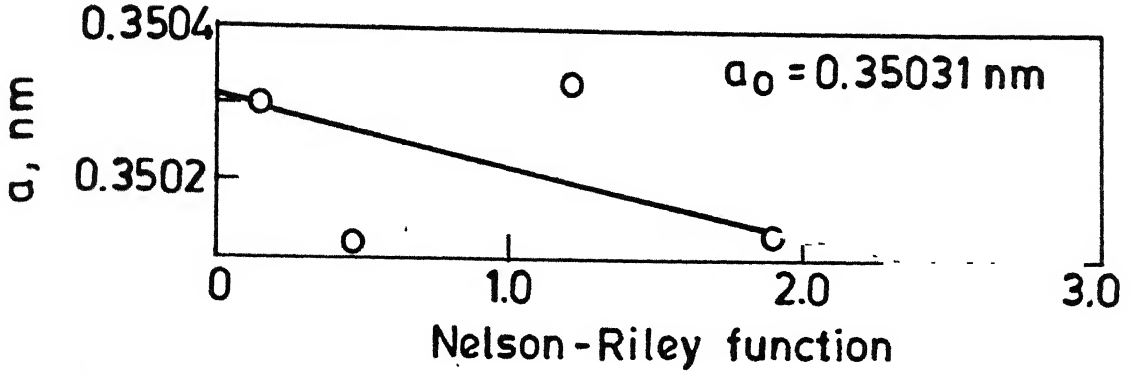

Fig. 5.5.2 Lattice parameter of pracipitated phase of sample aged at 750°C for 310 hrs.

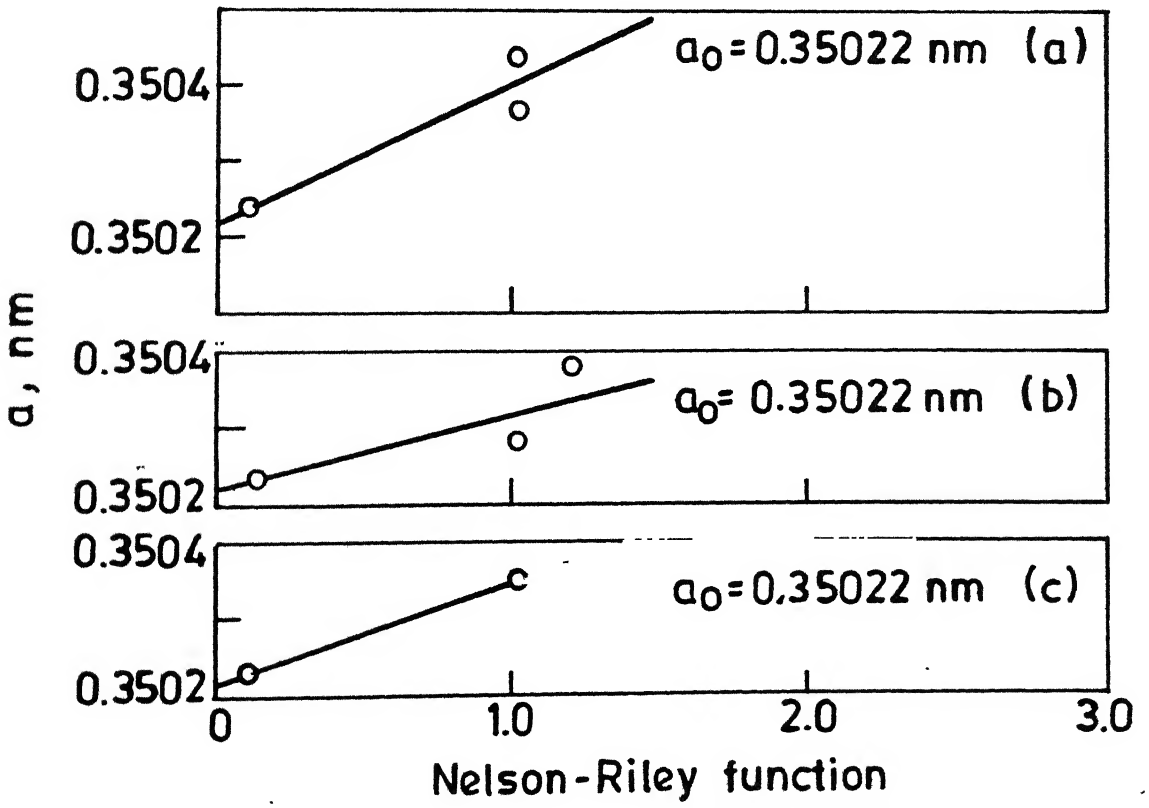

Fig. 5.5.3 Lattice parameter of precipitated phase of sample aged at 650°C for (a) 92 hrs (b) 165 hrs (c) 198 hrs.

Table 5.5.2 'a' Values of Precipitated β_1-Ni_3Si Phase

Temp (°C)	Time	Lattice Parameter (nm)
850°C	38 hrs.	0.35022
750°C	310 hrs.	0.35031
650°C	92 hrs.	0.35022
	165 hrs.	0.35022
	198 hrs.	0.35022

5.6 Hardening Effect due to Precipitation

Microhardness changes in the sample due to aging are shown in Figure 4.1.3. It shows that at 750°C, there is no hardening effect in fact the matrix starts softening due to the depletion of silicon. At 750°C, the temperature is so high that even during aircooling precipitation has taken place in the matrix and the precipitates quickly coarsen so that there is no hardening effect. This is demonstrated as a fact that specimens water quenched from homogenisation temperature has much higher hardness than those which were air cooled.

Similar behaviour is observed at 700°C of aging. However, because of lower rate of precipitation slight hardening effect is observed.

Specimens were water quenched from homogenisation temperature in order to prevent precipitation during aircooling. These were then aged at 650°C as a function of time. Aging at 650°C clearly gives considerable increase in strength. However, it starts softening only after 4 hrs. It clearly shows that in this system hardening effect can be observed but at a lower temperature. The lack of appreciable hardening by silicon is most likely due to the small mismatch of 0.45% in this system.

Chapter VI

Summary and Conclusions

(1) The lattice parameter of Ni-14 at. % Si alloy has been measured experimentally and was found to be in good agreement with the published results.

(2) The solution treated Ni-14 at. % Si alloy has been aged at 850°C for 20 and 38 hrs., at 750°C for 1, 2, 10, 150 and 310 hrs., at 700°C for 1, 2, 4, 10 and 40 hrs., at 650°C for 92, 165 and 198 hrs. and at 600°C for 22 and 85 hrs. and their lattice parameters were measured.

(3) The lattice parameters approaches a constant value after 40 hrs. at 700°C and after 150 hrs. at 750°C. The lattice parameters of the matrix phase and the precipitate, Ni_3Si have been determined at 850°C for 38 hrs., at 750°C for 310 hrs., at 650°C for 92, 165 and 198 hrs.

(4) From the results of aged samples, the solvus line has been determined which agrees very well with available data.

(5) The analysis of solvus curve gives a value of -351 cal/mole for the standard enthalpy of formation of compound $Ni_{0.773}Si_{0.227}$.

(6) The solid solution hardening found in this investigation do not confirm that elements having same electronic structure should produce same hardening effect. However, it was observed that hardening effect depend on atomic percent of the alloying element in tetravalent elements (Si, Ge, Sn).

(7) The lattice parameter of Ni_3Si has been measured from the results of aged samples. The values ranging between 0.35022 and 0.35031 nm is in good agreement with the published results.

(8) The kinetics of precipitation has been studied. It follows the Johnson-Mehl type of equation. The slope 'n' is found to be 0.83 at all aging times and temperatures. The value of K is found to be 2.4×10^{-4}. The result shows that same mechanism is valid at all temperatures and for entire time ranges. Metastable phases do not form during precipitation.

(9) The c-curve has been established which was found to be in good agreement with the available results.

(10) The precipitation hardening effect was found below 650°C. Precipitation at higher temperature is so fast that it cannot be suppressed by aircooling. Hardening of aircooled sample and 1 hr. aging at 700°C leads only a slight increase, while the hardening of aircooled sample and aged at 750°C for 1 hr. did not observed. However, aging at 650°C of quenched sample for small times upto 7 hrs. shows an increase in hardness.

References

(1) B. Stoughton, A. Butts and A.N. Bounds, Engineering Metallurgy, McGraw-Hill Book Company, Inc., 1953.

(2) P.K. Rastogi and A.J. Ardell, Acta Met., 19(4), 1971.

(3) M. Okamoto, Nippon Kinzoku Gakkai-Shi, 2, 1938, 544-551.

(4) A. Osawa and M. Okamoto, Nippon Kinzoku Gakkai-Shi, 2, 1938, 378-388.

(5) K. Kusumoto, Nippon Kinzoku Gakkai-Shi, 2, 1938, 617-619.

(6) N.F. Lashko, Doklady Akad. Nauk SSSR,, 81, 1951, 605-607.

(7) A.K. Chakraborty and Erhard Hornbogen, Z. Metallkunde, 1966, 57(1), 28-33.

(8) T. Suzuki and Y. Oya, Z. Metallkunde, 1983, 74(1), 21-24.

(9) O. Naguchi, Y. Oya and T. Suzuki, Met. Trans., 12A (1981), 1647.

(10) E. Hornbogen and M. Roth, Z. Metallkunde, 58, 842 (1967).

(11) A. Kelly and R.B. Nicholson, Prog. Mater. Sci., 10, 151, 158 ff, 178 ff (1963).

(12) P.K. Rastogi and A.J. Ardell, Acta Met., 17(5), 1969.

(13) P.H. Thornton and R.G. Davies, Met. Trans., 1970, 1, 549-50.

(14) N.S. Stoloff and R.G. Davies, Phil. Mag., 1965, Vol. 12, pp. 297-304.

(15) Metals Hand Book, Vol. 1, 8th Ed., 1972.

(16) A.K. Jena and I. Rambrahama, to be published.

(17) Hanson and Anderko, Constitution of Binary Alloys; Material Science and Engineering Series, 2nd Ed., 1958, pp. 1039-42.

(18) W. Klement, Jr., Can. J. Phys., 40, 1962, 1397-1400.

(19) W. Guertler and G. Tammann, Z. Anorg. Chem., 49, 1906, 93-112.

(20) K. Iwase and M. Okamoto, Science Repts. Tohoku Imp. Univ., K. Honda Annio, Vol. 1936, pp. 777-792.

(21) A.C. Fossyth and R.L. Dowdell, Trans. AIME, 137, 1940, 373-387.

(22) K. Ruttewit and G. Masing, Z. Metallkd., 32, 1940, 60.

(23) R.P. Ram and Suraj Bhan, Z. Metallkd., 1975, 66(9), 521-524.

(24) Labaili, Soltane; Haner. Thibouls, Sylvaine Z. Metallkd., 1984, 75(10), 764-70.

(25) Lutskaya, L.F. and Gel'd, P.V., Izv. Akad. Nauk. SSSR, Neorg. Mater., 1977, 13(2), 376-7.

(26) G. Pilstrom, Acta Chem. Scand., 15, 1961, 893-902.

(27) G.S. Saini, L.D. Calvert and J.B. Toylor, Can. J. Chem., 42, 1964, 1511-1517.

(28) K. Toman, Acta Cryst., 5, 1952, 329-331.

(29) B. Boren, Arkiv. Kemi, Mineral-Geol., 11A, 1933, 22-23.

(30) K. Schubert and H. Pfisterer, Z. Metallkd., 41, 1950, 438.

(31) K. Toman, Acta Cryst., 4, 1951, 462-464.

(32) A. Wittman, K.O. Burger and H. Nowotny, Monatsh. Chem., 92, 1961, 961-966.

(33) W.R. Johnson and M. Hansen, AF Technical Report 6383, 1951.

(34) W. Oelson and H.O.V. Samson-Himmelstjerna, Dusseldorf, 18, 1936, 131-133.

(35) E.B. Badtiev, O.C. Petrushova, L.A. Pantelle and I. Monov, Sor. Khim., 15 (1974), 367.

(36) G.S. Gardiner, J. Hummel, A. Rahnema, M.A. Ruggiero and J.W. Rutter, J. Cryst. Growth, 58 (1982), 522-526.

(37) A.J. Ardell, U.S. Atomic Energy Comm., 1968, CAL-T-221-39, 28 pp.

(38) P.K. Rastogi, U.S. Atomic Energy Comm., 1969, CAL-T-221-78, 53 pp.

(39) P.K. Rastogi, J. Appl. Phys., 1970, 41(10), 4243-4.

(40) P.K. Rastogi and A.J. Ardell, Acta Met., 1971, 19(4), 321-30.

(41) M.A. Dvorack and S. Polat, Scr. Metall., 1984, 18(12), 1395-9.

(42) P.K. Rastogi and A.J. Ardell, Acta Met., 1969, 17(5), 595-602.

(43) Barker, William; Evans, Thomas Ernest; Williams Kieth, J. Brist. Corr. J., 1970, 5(2), 76-80.

(44) Yoshida, Hidehiko; Takeuchi, Shin; Fukuzawa, Yasumitsu Nippon Kinzoku Gakkai-Shi (J. of Japan Inst. of Metals), 1970, 34(8), 821-5.

(45) S.G. Khayutin and I.V. Meshchaninov, Fiz. Met. Metalloved., Jan. 1980, 49(1), 158-165.

(46) Y. Oya, T. Suzuki and O. Shouichi, Metall. Trans. A, 1984, 15A(1), 173-81.

(47) High Voltage Electron Microsc., Proc. Int. Conf., 3rd ed., (Pub. 1974), 268-72.

(48) N.S. Stoloff and R.G. Davies, Prog. Mater. Sci., 1966, Vol. 13, p. 3.

(49) Scr. Metall., Apr. 1985, 19(4), 551-56.

(50) A.K. Chakraborty and E. Hornbogen, Z. Metallkd., 58(i) (1967), 46-49.

(51) N.V. Ageev, L.N. Guseva and I.V. Egiz, Izv. Akad. Nauk. SSSR, Metal., 1969, (3), 112-118.

(52) G.V. Seregin, Y.F. Ivanov and V.F. Sukhovarov, Fiz. Met. Metalloved., Dec. 1979, 48(6), 1235-43.

(53) A.L. Berezina, A.E. Ferekos and K.V. Chuistov, Metallofizika, 1974, 50, 52-8.

(54) Fiz. Met. Metalloved., Aug. 1980, 50(2), 333-38.

(55) G.N. Flint and W. Barker, Soc. Chem. Ind. (London), Chem. Eng. Group, Proc. 43, FB1-10 (1964).

(56) C.R. Acad. Sci., Ser. C, 1974, 279(3), 91-94.

(57) L. Beaunier, C. Chefi, M. Froment and C. Vignaud, Met. Corros., Proc. Int. Congr. Met. Corros., 8th, 1981, 1, 50-55.

(58) P. Kumar, Mater. Res. Soc. Symp. Proc., 1985, 39, 537-54.

(59) J. Microsc. Spectrosc. Electron, 1978, 3(3), 265-70.

(60) G. Lerang, L. Minel, S. Bouquet and J.P. Langeron, Surf. Sci., 1985, 152-153(2), 947-56.

(61) Proc. Electrochem. Soc., 1976, 77-1, 576-84.

(62) V.E. Krivosheya, V.V. Stepanov and A.P. Vochkanov, Zashchita Metallov, Jan.-Feb. 1970, 6(1), 29-30.

(63) Khim. Neft. Mashinostr., 1976, (1), 25-8.

(64) B.D. Cullity, Elements of X-ray Diffraction, Addison-Wesley Pub. Company, Inc., 1956.

(65) N.J. Grant and R.M.N. Pelloux, Trans. Met. Soc. AIME, 218, 1960, p. 282.

(66) A.K. Jena and R.R. Nagaragan, work to be published.

(67) J.W. Christian, The Theorem of Transformations in Metals and Alloys, Pergamon Press, London, 1965.

page 1

APPENDIX 1

PROGRAM FOR THE CALCULATION OF 2θ VALUES OF PURE NICKEL

```
      REAL WCUKA(3)
      INTEGER IH(7),IK(7),IL(7)
      DATA PRINT/'LP:'/
      DATA IPLANE/7/
      DATA INCUKA/3/
      DATA PI/3.1415926534/
      DATA A/3.5239/
      DATA WCUKA/1.5417A,1.54051,1.51433/
      DATA IH/1,2,2,3,2,4,3/
      DATA IK/1,0,2,1,2,0,3/
      DATA IL/1,0,0,1,2,2,1/
      OPEN(UNIT=PRINT,DEVICE='DSK',FILE='T2CALC.INP')
      DO 10 IPLANE=1,IPLANE
      DO 20 INCUKA=1,INCUKA
      D=A/(1/SQRT(FLOAT(IH(IPLANE)*IH(IPLANE)+IK(IPLANE)*IK(IPLANE)+IL
     1 (IPLANE)*IL(IPLANE))))
      T2CALC=ASIN(0.5*WCUKA(INCUKA)/D)*360.0/PI
      WRITE(PRINT,*) T2CALC
   20 CONTINUE
   10 CONTINUE
      STOP
      END
```

PROGRAM FOR THE DETERMINATION OF LATTICE PARAMETER
BY THE LEAST SQUARE METHOD

page 1

```
      REAL ...(21),ERRV(21),...(21),T2CALC(7,3),T2HIST(7,3)
      REAL T2PURE(7,3),T2PV(21),WCUKA(3)
      INTEGER IH(7),IK(7),IL(7)
      DATA INP0/20/
      DATA INP1/21/
      DATA INP2/22/
      DATA NOUT/35/
      DATA NOUTE/33/
      DATA NPLANE/7/
      DATA NWCUKA/3/
      DATA EPSILN/0.10E-02/
      DATA PI/3.14159265/
      DATA WCUKA/1.54173,1.54051,1.54433/
      DATA IH/1,2,2,3,2,4,3/
      DATA IK/1,0,2,1,2,0,3/
      DATA IL/1,0,0,1,2,0,1/
      OPEN(UNIT=INP0,DEVICE='DSK',FILE='T2CALC.TMP')
      OPEN(UNIT=INP1,DEVICE='DSK',FILE='PURE1.TMP')
      OPEN(UNIT=INP2,DEVICE='DSK',FILE='HIST.TMP')
      OPEN(UNIT=NOUT,DEVICE='DSK',FILE='APMAP.OUT')
      OPEN(UNIT=NOUTE,DEVICE='DSK',FILE='T2PERR.OUT')
      READ(INP0,*)((T2CALC(IPLANE,IWCUKA),IWCUKA=1,NWCUKA),IPLANE=1,
     1           NPLANE)
10    CONTINUE
      READ(INP1,*,END=20) IPLANE
      READ(INP1,*,END=20) (T2PURE(IPLANE,IWCUKA),IWCUKA=1,NWCUKA)
      GO TO 10
20    CONTINUE
      READ(INP2,*,END=30) IPLANE
      READ(INP2,*,END=30) (T2HIST(IPLANE,IWCUKA),IWCUKA=1,NWCUKA)
      GO TO 20
30    CONTINUE
      NWM1=NWCUKA-1
      NV=0
      DO 80 IPLANE=1,NPLANE
      DO 60 IWCUKA=1,NWCUKA
      T2=T2PURE(IPLANE,IWCUKA)
      IF(T2.LT.EPSILN)GO TO 60
      NV=NV+1
      T2PV(NV)=T2
      ERRV(NV)=T2-T2CALC(IPLANE,IWCUKA)
60    CONTINUE
80    CONTINUE
      IPLANE=NV
100   CONTINUE
      IWCUKA=1
      DO 120 IM=2,IPLANE
      IF(T2PV(IM-1).GE.T2PV(IM)) GO TO 120
      T2=T2PV(IM-1)
      T2PV(IM-1)=T2PV(IM)
      T2PV(IM)=T2
      T2=ERRV(IM-1)
      ERRV(IM-1)=ERRV(IM)
      ERRV(IM)=T2
      IWCUKA=IM
120   CONTINUE
      IPLANE=IWCUKA-1
      IF(IPLANE.GT.1) GO TO 100
      DO 140 IM=1,NV
      WRITE(NOUTE,*)T2PV(IM),ERRV(IM)
140   CONTINUE
      WRITE(NOUT,1022) (WCUKA(IWM1+1),IWM1,IWM1=0,NWM1)
      N=0
      DO 300 IPLANE=1,NPLANE
      DO 200 IWCUKA=1,NWCUKA
      T2=T2HIST(IPLANE,IWCUKA)
      IF(T2.LT.EPSILN) GO TO 200
      IM=2
160   CONTINUE
      IF(T2.LT.T2PV(IM)) GO TO 180
      IM=IM+1
      IF(IM.LT.NV) GO TO 160
180   CONTINUE
      ERROR=ERRV(IM)+(ERRV(IM)-ERRV(IM-1))*(T2-T2PV(IM))/
```

```
1          (T2PV(I-1)-T2PV(IM-1))
           T2CORR=T2-T2RHR
           D=T2CORR*FOI/3E5
           A=A+SUMA(I)*COSA/SIN(T)
           F=F+((SUMA(I)*IE(IPLANE)*TI(IPLANE)+IE(IPLANE)*IA(IPLANE)+
                IA(IPLANE)*IB(IPLANE)))
           F=F*COS(T)*COS(T)*(1.0/SIN(T)+1.0/T)
           I=I+1
           T(I)=T
           F(I)=F
           IM=IMAX-1
           WRITE(6,10+1)IPLANE,IE(IPLANE),IA(IPLANE),IB(IPLANE),TH,
          1      T2,CORR,T2CORR,D,A,F,VR
2          CALL EXIT
3          CALL PLOTS
           SUMA=0.0
           SUMF=0.0
           SUMA2=0.0
           SUMF2=0.0
           SUMAF=0.0
           DO 32 I=1,IM
           SUMA=SUMA+A(I)
           SUMF=SUMF+FCORR(I)
           SUMA2=SUMA2+A(I)*A(I)
           SUMF2=SUMF2+FCORR(I)*FCORR(I)
           SUMAF=SUMAF+A(I)*FCORR(I)
32         CONTINUE
           RIM=FLOAT(IM)
           SLOPE=(RIM*SUMAF-SUMA*SUMF)/(RIM*SUMA2-SUMA*SUMA)
           AINT=(SUMA-SLOPE*SUMF)/RIM
           CORR=100.0*(RIM*SUMAF-SUMA*SUMF)/SQRT((RIM*SUMA2-SUMA*SUMA)
          1      *(RIM*SUMF2-SUMF*SUMF))
           WRITE(IOUT,1006) SLOPE,AINT,CORR
           STOP
1002       FORMAT(9(1X/),3(34X,'O'/15X,'A',7X,'=',F9.6,
          1      'A'/16X,'Cu KA',11/),5(1X/),10X,'PLANE',2X,'( H K L )',
          2      2X,'MCu',4X,'12NTST',6X,'ERROR',6X,'T2CORR',9X,'D',
          3      11X,'A',5X,'M',K, FM,'/1X)
1004       FORMAT(1X/10X,I3,4X,'(',3I2,' )',2X,'KA',I1,F12.6,F11.6,F12.6,
          1      F13.9,F10.6,F10.6)
1006       FORMAT(5(1X/),6X,'RESULT :'/5X,6('=')/1X/17X,'SLOPE',10X,'=',
          1      F16.8/1X/17X,'A - INTERCEPT  =',F16.8/1X/15X,
          2      '( CORRELATION     =',F10.3,' % )')
           END
```

98040

Thesis
669.7332 Date Slip 98040
V823p

This book is to be returned on the date last stamped.

....	..... .
....	.....
.. ..	....
....	... ...
....	.. ..
.. ..	.....
. ...	.....
....	.....
....	....
.....	....
.....	....
... .	. . ..

ME - 1986 - M - BAN - PRE